Global and Planetary Change 182 (2019) 103027

Contents lists available at ScienceDirect

Global and Planetary Change

journal homepage: www.elsevier.com/locate/gloplacha

Research article

Transfer of deformation during indentation: Inferences from the post-middle Miocene evolution of the Dinarides

Marianne van Unen[a,b,*], Liviu Matenco[a], Vedad Demir[c], Fadi Henri Nader[b], Romain Darnault[b], Oleg Mandic[d]

[a] Faculty of Geosciences, Utrecht University, Utrecht, the Netherlands
[b] IFP Energies Nouvelles, Rueil-Malmaison, France
[c] Federal Institute for Geology, Sarajevo, Bosnia and Herzegovina
[d] Natural History Museum Vienna, Vienna, Austria

ARTICLE INFO

Keywords:
Continental indentation
Continental subduction
Continental restraining bends or step-overs
Adriatic microplate
Dinarides

ABSTRACT

Understanding the structural and kinematic effects of indentation is still debated due to the large number of competing mechanisms associated with the complex orogenic build-up. Among the many examples available worldwide, the evolution of the Adriatic continental microplate in the Mediterranean domain provides one of the best places to understand the mechanics of indentation. This understanding is hampered by the lack of structural and kinematic data in the Dinarides, an orogen situated at the critical transition between the Alps, Albanides and Hellenides, and across the Adriatic margin of the Apennines. We have studied the less known area of the central and south-eastern Dinarides by focussing on collecting a new kinematic dataset for structures formed during the Adriatic indentation, which postdates the main Late Jurassic – Paleogene orogenic structuration. Our results are in agreement with previous interpretations of an early-middle Miocene period of extension that affected the entire orogen across its strike and is incompatible with indentation effects in the studied parts of the Dinarides. More importantly, we demonstrate for the first time that the post- middle Miocene Dinarides deformation was characterized by a coherent regional system of large offset dextral strike-slip faults, which transfer gradually their offsets to thrusts and high-angle reverse faults. The overall deformation transfer mechanism can be described as a special class of continental restraining bends or stepovers, whose geometry is controlled by rheological distribution. The integration of our results in the larger geodynamic context shows that the post-middle Miocene Dinarides fault system accommodates the differential motion between the N- to NE-wards Adriatic indentation and the rapid S- to SW- ward movement of a Hellenides area situated SE of the Kefalonia Fault, driven by the Aegean slab-roll back.

1. Introduction

The architecture of mountain belts is often controlled by the evolution and dynamics of subducted slabs during the final stages of continental collision (e.g., Andrić et al., 2018; Burov et al., 2014; Duretz and Gerya, 2013; Faccenna et al., 2014; Matenco et al., 2010). The term indentation has been used to define the collisional mechanics of a small continental plate flanked by subduction zones, creating significant crustal thickening and/or lateral escape of blocks against strike-slip faults, facilitated by rheological strength contrasts or changes in subduction mechanics, such as lateral slab retreat (e.g., Davy and Cobbold, 1988; Molnar and Tapponnier, 1975; Regard et al., 2005). Understanding the structural and kinematic effects of indentation has been a subject of debate due to the large number of competing mechanism, ranging from crustal and lithospheric thickening and folding, lower crustal flow, lateral extrusion, to oblique oceanic or continental subduction (e.g., Houseman and England, 1993; Meissner and Mooney, 1998; Molnar and Tapponnier, 1975; Rosenberg et al., 2007; Smit et al., 2013; van Gelder et al., 2017). In many situations observed in the India-Asia or Mediterranean collision systems, indentation is associated with the evolution of opposite dipping subduction zones situated at the margins of the continental plate fragment, where a lateral transfer of contractional deformation across multiple orogens is observed (Doglioni et al., 2007; Faccenna et al., 2014; Faccenna et al., 2004; Jolivet et al., 2018). While the significant thickening of the continental fragments is usually described as indentation, the same convergence

* Corresponding author at: Tectonics Group, Department of Earth Sciences, Utrecht University, PO Box 80021, 3508 TA Utrecht, the Netherlands.
E-mail address: m.vanunen@uu.nl (M. van Unen).

https://doi.org/10.1016/j.gloplacha.2019.103027
Received 6 February 2019; Received in revised form 15 August 2019; Accepted 29 August 2019
Available online 30 August 2019
0921-8181/

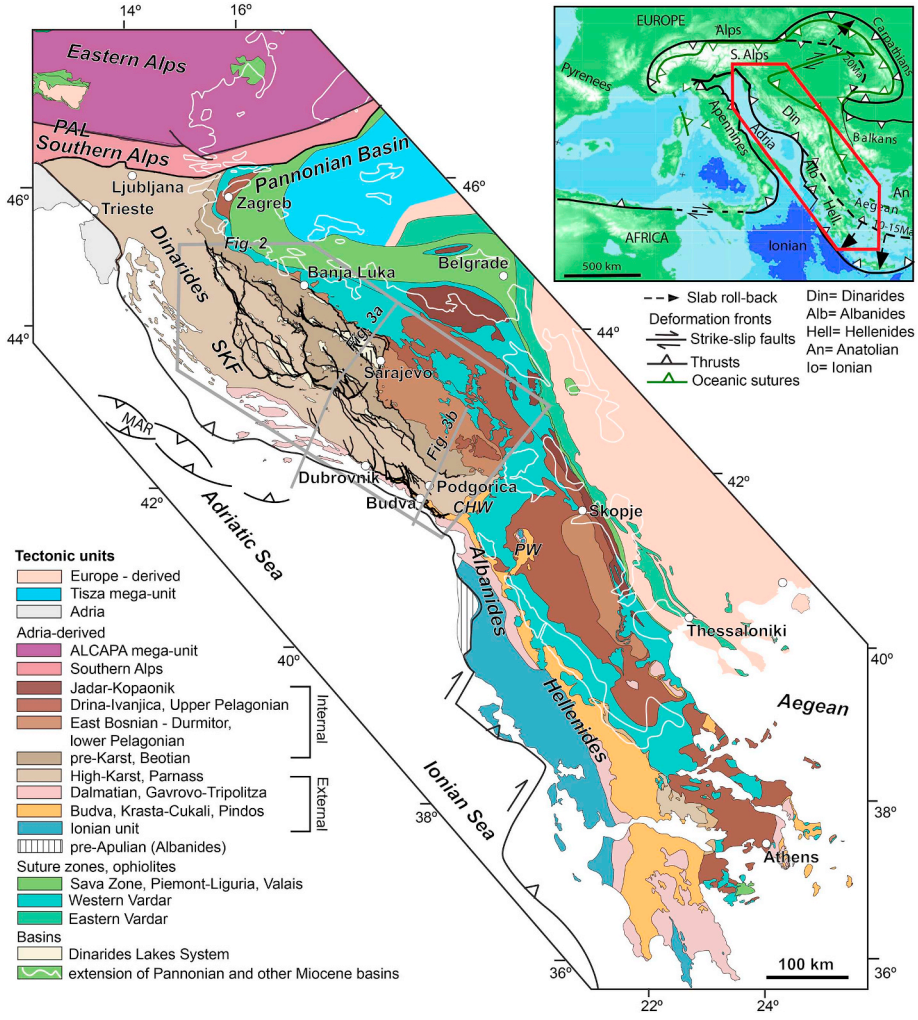

Fig. 1. Tectonic map of the external parts of the Dinarides, Albanides and Hellenides, as well as the neighbouring parts of Pannonian Basin, Southern and Eastern Alps (after Schmid et al., 2008; Schmid et al., 2011). In the Dinarides, the map is overlain by the post- 9 Ma fault system depicted in this study and by Miocene basins belonging to the Dinarides Lake System (Harzhauser and Mandic, 2008; Mandic et al., 2012). The grey polygon is the location of the map in Fig. 2. The grey lines are the locations of the cross-sections in Fig. 3a, b. The map in the upper right corner is the localisation of the tectonic map in the larger European orogenic context. Din = Dinarides; Alb = Albanides; Hell = Hellenides; An = Anatolia; S. Alps = Southern Alps; PAL = Peri – Adriatic Lineament; SKF = Split – Karlovac Fault; MAR = Middle Adriatic Ridge. Dashed lines are locations of the orogenic front in the Carpathians and Aegean domain at 20 and 15 Ma, respectively (modified after Wortel and Spakman, 2000).

process is described laterally in the opposite polarity subduction systems as oceanic or continental subduction (Faccenna and Becker, 2010; Jolivet et al., 2018; Munteanu et al., 2014; Peral et al., 2018; Regard et al., 2005). This contrast leads to a situation where a clear process-based discrimination between subduction and indentation, based on observations in transition zones, is too often unclear. In particular, kinematic studies are required in such transitional zones to discriminate processes and understand indentation effects.

One typical example of the interplay between indentation, opposite polarity subduction zones and associated deep mantle processes is the one observed for the post-Paleogene evolution of the Adriatic micro-plate, which is situated between the opposite polarity orogenic systems of the Alps and the ones of the Dinarides and Apennines (Fig. 1, Handy et al., 2014; Király et al., 2018; Le Breton et al., 2017; Ustaszewski et al., 2008). The kinematics and timing of deformation is relatively well understood in the rapid transition zone between the Alps and Apennines (e.g., Bertotti et al., 2006; Handy et al., 2010; Picotti and Pazzaglia, 2008; Schmid et al., 2017). In contrast, the balance between the Alps-Dinarides subduction polarity change, Adria indentation and subduction of the Adriatic plate in the Dinarides (Fig. 1) is much less understood (e.g., Bennett et al., 2008; Kissling et al., 2006; Schmid et al., 2008; Šumanovac et al., 2017). This understanding is hampered in particular by the poor knowledge of the post-Paleogene kinematics in the external Dinarides (Fig. 1). This 700 km long orogen connects the intense post-Paleogene and active deformation presently observed in the Southern Alps, defined as Adriatic indentation, with the active subduction and retreat of the Aegean slab that still drives the evolution of the Albanides – Hellenides orogenic system (e.g., Handy et al., 2019; Jolivet and Brun, 2010; Jolivet et al., 2015; Schmid et al., 2008; van Gelder et al., 2017). The Adriatic indentation was associated in the Southern Alps and internal part of the Dinarides with thrusting, dextral movements and/or extrusions along the Peri-Adriatic Lineament (e.g., Fodor et al., 1998; Frisch et al., 2000; Tomljenović and Csontos, 2001; Ustaszewski et al., 2014; Vrabec et al., 2006; Wölfler et al., 2011; Žibret and Vrabec, 2016). In contrast, there is almost no kinematic and timing documentation available for structures in the central and south-eastern part of the external Dinarides that would explain the present-day intense seismicity, crustal stress pattern and the up to 5 mm/yr N- to NE-ward movement with respect to stable Europe detected by GPS studies (Bennett et al., 2008; Caporali et al., 2009; Grenerczy et al., 2005; Heidbach et al., 2018; Métois et al., 2015; Pinter et al., 2005). This lack of data renders all previously inferred large-scale (up to 100 km) motions along various structures in the external part of the Dinarides, such as the NNW-SSE oriented dextral strike-slip Split-Karlovac Fault System (Fig. 1, e.g., Chorowicz, 2016; Ustaszewski et al., 2008) and resulting reconstructions of Adriatic indentation (e.g., Picha, 2002) as highly speculative. Therefore, a quantitative understanding of the effects and mechanics of the N-ward Adriatic indentation and its relationship with the inherited NW-SE oriented Dinarides structure is still not available.

We aim to fill this gap in regional and process-oriented knowledge by quantifying the post-Paleogene kinematics and timing of structures associated with the indentation of the Adriatic continental micro-plate and its continental subduction observed in the external parts of the Dinarides. We have collected a new kinematic dataset for structures

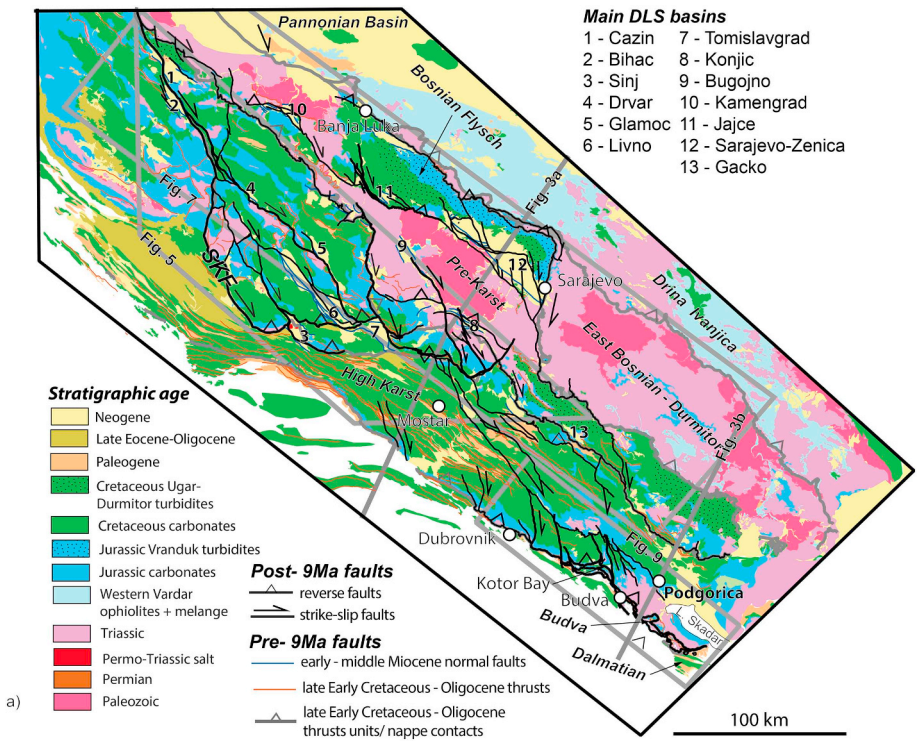

Fig. 2. Geological map of the central and south-eastern part of the Dinarides (simplified from 1:100,000 maps of former Yugoslavia – OGK, Osnova Geoloska Karta) overlaid by the post- 9 Ma fault system kinematically mapped in this study and the major nappe contacts depicted in Fig. 1. Note also the location of the main Miocene Dinarides Lake System (DLS) basins (Harzhauser and Mandic, 2008; Mandic et al., 2012). Early-middle Miocene faults were displayed and correlated only in the area covered by the Miocene basins, while Eocene-Oligocene faults are taken from the above mentioned geological maps and their interpretation is based only on stratigraphic juxtapositions. Grey polygons are the locations of maps in Figs. 5, 7 and 9. The grey lines are the locations of the cross-sections in Fig. 3a, b. SKF = Split – Karlovac Fault.

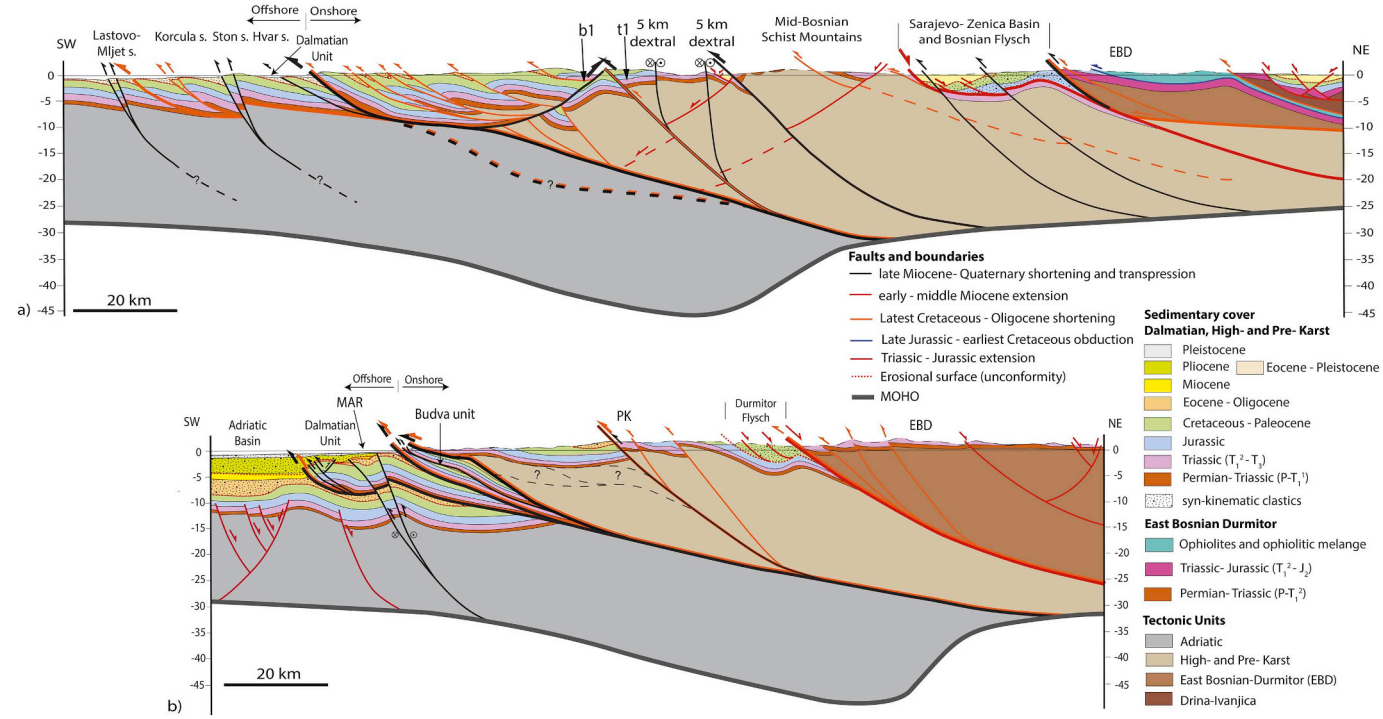

Fig. 3. Cross-section over the external Dinarides (reinterpreted after van Unen et al., 2019; van Unen, 2019). The locations of the cross-sections are displayed in Figs. 1, 2, 5, 7 and 9. a) Kinematically controlled cross-section in the central part of the external Dinarides. Note the superposition of deformation between older late Jurassic – Eocene thrusts, early-middle Miocene normal faults and post- middle Miocene structures. t1 and b1 are a thrust and backthrust discussed in the text and displayed also in Fig. 7a; b) Kinematically controlled cross-section located in the SE part of the Dinarides. Details of the seismic interpretation and its alternatives in the offshore part are available elsewhere (Bega, 2015; van Unen, 2019). MAR = Middle Adriatic Ridge. The quantitative restoration of this cross-section is available in Fig. 11.

that postdate the main Late Jurassic – Paleogene orogenic evolution in the central and south-eastern Dinarides (Fig. 2). We use one critical timing indicator not previously accounted for, which is the deformation of Miocene sediments deposited during the development of the Dinarides Lake System. This system is an endemic and isolated group of intramontane lakes that overlies the previous orogenic structure and whose areal extent was enhanced by the Miocene Climatic Optimum (Figs. 1 and 2, Harzhauser and Mandic, 2008; Harzhauser et al., 2011; Mandic et al., 2012). Given the unusual large extent of our studied area, we have focused our observations to ultimately interpret only post- middle

Miocene large offset faults that affect the Dinarides Lake System sediments and can be followed regionally outside the Miocene basins. A quantification is achieved by the means of a field kinematic study correlated with cross-sections and restoration, available information on timing, orogenic structure and evolution, seismicity, crustal stress pattern and GPS motions. The results are discussed in the context of characterizing deformation mechanics and understanding regional effects associated with the Adriatic indentation in the larger framework of the neighbouring Southern Alps, Albanides, Hellenides and Apennines orogens.

2. The Dinarides orogenic evolution and the Adriatic indentation

The Dinarides are part of a Mediterranean orogenic system that evolved during Mesozoic–Cenozoic times (Figs. 1 and 2). The opening of a northern branch of the Neotethys Ocean located between Adriatic- and European- derived continental units took place during the Middle Triassic (e.g., Schmid et al., 2008; Stampfli and Borel, 2002). Structures associated with this opening are rather scarce in the presently observed Dinarides nappe stack, but a NE-SW direction of extension has been inferred in the internal Dinarides and the Budva Unit of Montenegro (e.g., Toljić et al., 2013; van Unen et al., 2019). The Neotethys opening in the Dinarides was associated with widespread rifting magmatism and the subsequent formation of a wide passive Adriatic continental margin (e.g., Dimitrijevic, 2001; Pamic, 1984). While the proximal part of this continental margin (SW-wards in Fig. 2) recorded almost continuous and thick Triassic–Paleocene shallow-water carbonate sedimentation (in the Dalmatian, High-Karst and Pre-Karst units in Figs. 1–4), its distal parts (NE-wards in Fig. 2) recorded gradual subsidence and deepening of a carbonate to marine pelagic facies during Middle Triassic – Lower Jurassic times (Fig. 4, Korbar, 2009; Schefer, 2010; van Gelder et al., 2015; Vlahovic et al., 2005). The exception is the Middle Triassic formation of the external located Budva graben (Fig. 4b), subsequently incorporated in the orogenic nappe stack (Fig. 3b), which recorded continuous deep-water carbonatic to pelagic sedimentation until Cretaceous times, interrupting the spatial continuity of the Adriatic shallow-water carbonate sedimentation (Cadjenovic et al., 2008; Crne et al., 2011; Gorican, 1994; Vlahovic et al., 2005). Laterally, the Budva unit can be correlated to the SE with similar deep-water deposits located in the Krasta-Cukali and Pindos units of Albania and Greece, respectively, while rapidly pinching out NW-wards in the present Dinarides structure (Fig. 1, e.g., Korbar, 2009; Robertson and Shallo, 2000; Schmid et al., 2008).

2.1. Orogenic deformation in the Dinarides

The onset of the Middle Jurassic Neotethys oceanic subduction continued with a Late Jurassic–earliest Cretaceous obduction of the Western Vardar Ophiolitic unit over the Adriatic margin, which is observed by top- NW to WNW thrusting of ophiolites and associated ophiolitic melanges overlying in an upper structural position the internal-most units of the Dinarides (Fig. 1, e.g., Dimitrijević, 1997; Robertson et al., 2009; Schmid et al., 2008). Subduction continued during Cretaceous times and peaked with the latest Cretaceous–earliest Paleogene collision between Adriatic- and European- derived continental units that was associated with the formation of a suture zone at their contact (the Sava Zone, Fig. 1, Pamić, 2002; Toljić et al., 2018; Ustaszewski et al., 2009). Orogenic movements continued by renewed Eocene – Oligocene shortening, recorded with larger offsets in the external part of the Dinarides and with reduced amplitudes in more internal units (Andrić et al., 2017; Dimitrijević, 1997; Stojadinovic et al., 2017; Ustaszewski et al., 2010). All these Cretaceous – Paleogene orogenic deformations are characterized by NE-SW oriented contraction and have created the presently SW-ward verging Dinarides nappe stack (Figs. 2 and 3a,b). The peak deformation episodes were associated with the deposition of turbidites ("flysch" deposits) in the footwall of various thrusted units. The thickest deposition of such turbidites is observed in the Bosnian Flysch zone (Figs. 2 and 3), which is located in the footwall of the ophiolite-carrying East Bosnian – Durmitor unit and can be possibly correlated laterally with similar turbidites located in the footwall of the adjacent Southern Alps thrusting (the Tolmin Flysch, Dimitrijević, 1997; Goričan et al., 2012; Hrvatović and Pamić, 2005; Tari, 2002). The deposition of the Bosnian Flysch started during Late Jurassic times (the Vranduk Flysch) and continued with larger amounts during latest Cretaceous (Maastrichtian) times (the Ugar-Durmitor Flysch), while this deposition was locally interrupted by unconformities (Fig. 4, Dimitrijević, 1997; Hrvatović, 2006; Hrvatović and Pamić, 2005; Mikes et al., 2008; Schmid et al., 2008). Latest Cretaceous syn-depositional thrusting was documented in Ugar-Durmitor turbidites, associated with a NE-SW oriented shortening event (van Unen et al., 2019). In a more external position, the Eocene (-Oligocene?) thrusting of the High-Karst and Budva units was associated with a similarly oriented NE-SW shortening event that was coeval with the sedimentation of turbidites in their footwall, followed locally by the late Eocene – Oligocene deposition of a shallow-water to alluvial continental regressive sequence (Fig. 4, e.g., the Promina "molasse", Mrinjek, 1993; Tari and Mrinjek, 1994; Zupanič and Babić, 2011). The NE-SW oriented contraction style was strongly influenced by the inherited rheology, high amounts of thrusting and short-wavelength folding being observed in turbidite belts and deep-water sediments of the Budva zone, while lower amounts of thrusting and long-wavelengths folding being observed elsewhere in the dominantly shallow-water carbonates of the external Dinarides (Fig. 3, Andrić et al., 2018; van Unen et al., 2019).

These successive orogenic building episodes were followed by a period of early-middle Miocene extension that affected large areas of the Dinarides. This extension was widely observed along the NE contact with the Pannonian Basin, where the Sava Zone was reactivated along its entire strike by the creation of multiple extensional detachments (e.g., Ustaszewski et al., 2010; van Gelder et al., 2015). A bimodal NE-SW and NW-SE oriented extension affected also more external Dinarides areas, where it created many of the basins that are part of the Dinarides Lake System (Fig. 1, Andrić et al., 2017; Harzhauser et al., 2011; Mandic et al., 2012; van Unen et al., 2019). The 18 Ma onset of extensional deposition observed in these basins post-dates the ~20 Ma onset of back-arc extension observed in the neighbouring southern Pannonian Basin, interpreted to be driven by the roll-back of an orogenic slab situated at far distances from the Dinarides (i.e. the Carpathians slab, Fig. 1, de Leeuw et al., 2012; Horváth et al., 2015; Mandic et al., 2012; Pavelić and Kovačić, 2018). This onset also post-dates the Oligocene onset of extension observed in the south-eastern part of the Pannonian Basin, near the contact with the Carpathians units (e.g., Erak et al., 2017). In the Dinarides, the amounts of extension observed decreased after 15 Ma (when deposition in smaller basins like Sinj or Gacko terminated) and was still active until 14 Ma in the Sarajevo-Zenica Basin and until 13 Ma in the Livno and Tomislavgrad basins (Figs. 2 and 3a, de Leeuw et al., 2011; de Leeuw et al., 2010; Mandic et al., 2011; Sant et al., 2018). Extension peaked at ~15–14 Ma in the neighbouring Pannonian Basin over a 15 Ma transition from alluvial and lacustrine to marine deposition, while gradually expanding southwards until 12.8 Ma (Mandic et al., 2019a; Mandic et al., 2019b; Pavelić and Kovačić, 2018). Interrupted by a short contractional event at the transition between middle and late Miocene, the back-arc extension continued in the southern Pannonian Basin during the late Miocene until ~8 Ma, when the Carpathians subduction zone was locked and the associated thin-skinned shortening ceased (Balázs et al., 2016; Matenco et al., 2016; Matenco and Radivojević, 2012).

2.2. N- to NE-ward Adriatic indentation in the Dinarides and neighbouring areas

The onset of the N-ward motion and indentation of the Adriatic unit was recorded in the Southern Alps starting with the latest Oligocene –

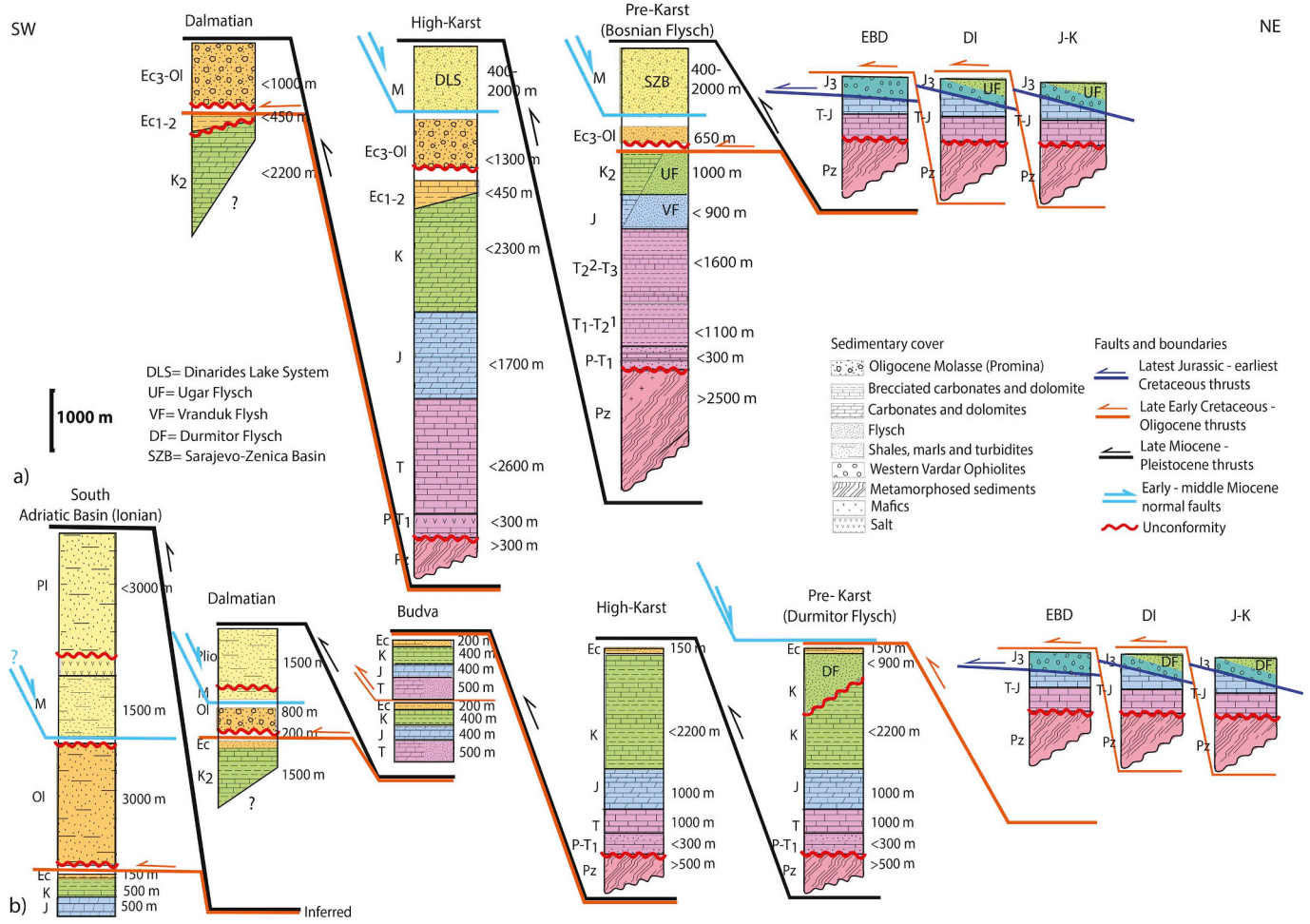

Fig. 4. Correlation of lithostratigraphic columns across various tectonic units in the external Dinarides, a) the central part of the Dinarides roughly along the trace of the cross-section in Fig. 3a; b) the SE part of the Dinarides roughly along the trace of the cross-section in Fig. 3b. All columns are simplified and correlated from surface mapping studies (1:100.000 maps of former Yugoslavia – OGK, Osnova Geoloska Karta), except the South Adriatic column that is derived from offshore wells (see Bega, 2015 for further details). Whenever outcropping, the Variscan basement is overlain by Permian – Lower Triassic continental deposits and/or evaporites. In the external part of Dinarides, upper Lower Triassic – Paleocene carbonates reach 2–3 km in cumulative thickness. Ages: Pl = Pliocene, Pl = Pliocene–Pleistocene, M = Miocene, Ec_{1-2} = lower-middle Eocene, Ec_3-Ol = upper Eocene – Oligocene, Ec = Eocene, K_2 = Upper Cretaceous, K = Cretaceous, J = Jurassic, J_3 = Upper Jurassic, T_3 = Upper Triassic, T_2^2 = upper Middle Triassic, T_2^1 = lower Middle Triassic, T_1 = Lower Triassic, P-T_1 = Permo–Triassic, P = Permian and Pz = (locally metamorphosed) Paleozoic.

early Miocene, and was associated with a lateral extrusion of the Eastern Alps into the Pannonian Basin starting at ~20 Ma that is still presently observed at a convergence rate of ~2–5 mm/yr (Grenerczy et al., 2005; Handy et al., 2010; Horváth et al., 2015; Ratschbacher et al., 1991). Strike-slip and contractional deformation is observed north and south of the right-lateral Peri-Adriatic Lineament, with larger amounts of upper crustal exhumation northwards (Fig. 1, Handy et al., 2014; Heberer et al., 2017; Tomljenovic et al., 2008).

In the external Dinarides, the NNW-SSE oriented Split-Karlovac Fault (Figs. 1 and 2) is thought to be one of the major structures formed during the Adriatic indentation (e.g., Ustaszewski et al., 2008), although no kinematic or timing data were so far provided. GPS studies show a 4–5 mm/yr N- to NE- ward present-day movement of the Dinarides with respect to a stable European framework (Grenerczy et al., 2005; Pinter et al., 2005). Furthermore, moderate to strong earthquakes are distributed along many fault systems in the Dinarides (e.g., Herak et al., 2009; Ustaszewski et al., 2014), although the kinematics of these faults is largely unknown. The overall Adriatic indentation is thought to have been associated with its counter-clockwise rotation and (continental) subduction, indicated from a high-velocity anomaly observed during geophysical studies beneath the Dinarides (Bennett et al., 2008; Šumanovac and Dudjak, 2016; Šumanovac et al., 2017). Although debated, some of these studies have inferred that the subducting slab in the SE part of the Dinarides reaches depths of up to 450 km, while remaining at shallower levels NW-wards (Šumanovac et al., 2017).

Although reconstructions generally assume that indentation associated with subduction started in the Dinarides at the same ~20 Ma times as in the Alps (Le Breton et al., 2017), observations indicate different onset ages. Obviously, one cannot define an indentation mechanism in areas of the Dinarides and at times where the above described Miocene extension was observed. In more details, the age of the youngest E-W to NE-SW oriented Dinarides thrusts, folds and strike-slip faults located near the contact with or inside the Pannonian Basin is generally thought to post-date either the middle Miocene or the entire Miocene in the centre and north-west (e.g., Fodor et al., 2005; Tomljenović and Csontos, 2001; Tomljenovic et al., 2008; Ustaszewski et al., 2014), or started at around 8.8–8.0 Ma in the south-east (Matenco and Radivojević, 2012; Toljić et al., 2013). Sedimentation continued in some intramontane basins of the Dinarides Lake System during the late Miocene. In the Sarajevo-Zenica Basin (Fig. 2), normal faults were inverted by thrusting during a deformation event that was coeval and post-dated the deposition of a 700 m thick coarsening upwards succession (the Orlac conglomerates, see discussion in Andrić et al., 2017). Palynological data from the intercalated coal seams provide a good

stratigraphic correlation with the 8.8–5.4 Ma age of similar deposits found in the southern part of the Pannonian Basin (Magyar and Geary, 2012; Pantić et al., 1966). The Livno and Tomislavgrad Basin (Fig. 2) recorded two late Miocene sedimentation cycles divided by an unconformity, which are correlated with the Pannonian Basin stratigraphy at 11.6–8.8 Ma and 8.8–4.5 Ma (Magyar and Geary, 2012; Milojevic and Sunaric, 1962; Milojević and Sunarić, 1964; Pantić and Bešlagić, 1964). The first cycle follows the outline of the two basins, while the second one shows a splitting of depocenters that can be interpreted to be *syn*-kinematic with respect to contraction and transpression (de Leeuw et al., 2011; van Unen et al., 2019). The cessation of Dinarides lacustrine deposition occurred ~ 5 Ma, which correlates with a regional unconformity observed in the southern Pannonian Basin (Pavelić and Kovačić, 2018; Ustaszewski et al., 2014). All these observations and interpretations suggest that the regional onset of contraction/transpression in the Dinarides and the tectonic inversion in the southern Pannonian Basin started somewhere ~ 8.8–8.0 Ma. We will further refer to this overall deformation event as the post- 9 Ma Adriatic indentation in the Dinarides.

3. Methodology and approach

We have performed a kinematic study in the Pre-Karst, High Karst, Budva and Dalmatian units located in the external part of the Dinarides in an area ~450 km along and 80–150 km across the strike of the orogen (Figs. 2–10). This area benefits from the full coverage of 1:100.000 scale geological maps (OGK Former Yugoslavia), where faults geometry and timing of Triassic – Paleogene deformation was extensively describes from associated stratigraphic juxtapositions (e.g., Dimitrijević, 1997; Schmid et al., 2008 and references therein). In contrast, only few kinematic studies describing the post-Paleogene deformation at local scale were previously performed (Sarajevo – Zenica Basin, Fig. 2, and the structural transects in Fig. 3a, b, Andrić et al., 2017; van Unen et al., 2019).

Obviously, a detailed kinematic analysis characterizing the entire deformation history of such a large area cannot be obtained in one study. Therefore, we have specifically focused our study to understand the post- Paleogene kinematic history by using the deformation observed in the lower – middle Miocene sediments of the Dinarides Lake System as a key timing indicator to discriminate the latest deformation events from pre-dating tectonic episodes. We started from analysing the geological maps and major structures inferred by previous studies to define a preliminary regional pattern of faults affecting the entire external Dinarides. The field study focused initially on mapping the kinematics of structures affecting the Miocene basins. We continued the field study in the prolongation of these structures along their strike outside the basins, where they truncate in map view the inherited pre-Miocene nappe structure, by mapping their kinematics and superposition criteria with older deformation events, derived from cross-cutting or re-activation relationships. These pre-Miocene deformation events are known to a large extent from previous regional, structural and kinematic studies (Andrić et al., 2017; Dimitrijević, 1997; Schmid et al., 2008; Ustaszewski et al., 2010), including in the study area (Fig. 3a, b, van Unen et al., 2019). Particularly relevant is the NE-SW orientation of the Late-Cretaceous – Paleogene shortening defined by all these studies, which corresponds to the general NW-SE orogenic strike (Fig. 2). We have used this knowledge to discriminate the pre-Miocene kinematics from the significantly different character of the subsequent deformation. This discriminations becomes important in areas outside the Miocene basins, such as the SE-most area of Montenegro (Fig. 8), where Miocene sediments are often missing or their stratigraphic age is uncertain onshore (see discussion in Mikes et al., 2008). In this area we mapped in the onshore the youngest kinematic event observed by superposition criteria starting from the previously published deformation history of van Unen et al. (2019), correlated with available deformation observed by the interpretation of seismic lines in the offshore (Figs. 2 and 3b, Bega, 2015; van Unen, 2019).

We furthermore focused the kinematic study to characterize the kinematics of faults that display large offsets in map view (Figs. 2, 5, 7 and 9). These faults were initially identified to have large stratigraphic offset (vertical and/or horizontal) in the high-quality maps available and were confirmed or re-interpreted subsequently by field observations to be associated with large displacements (from hundreds of metres to 25 km) along faults or shear zones. We have taken most measurements in such major shear zones, generally characterized by the development of wide fault gouge foliations or high density faults

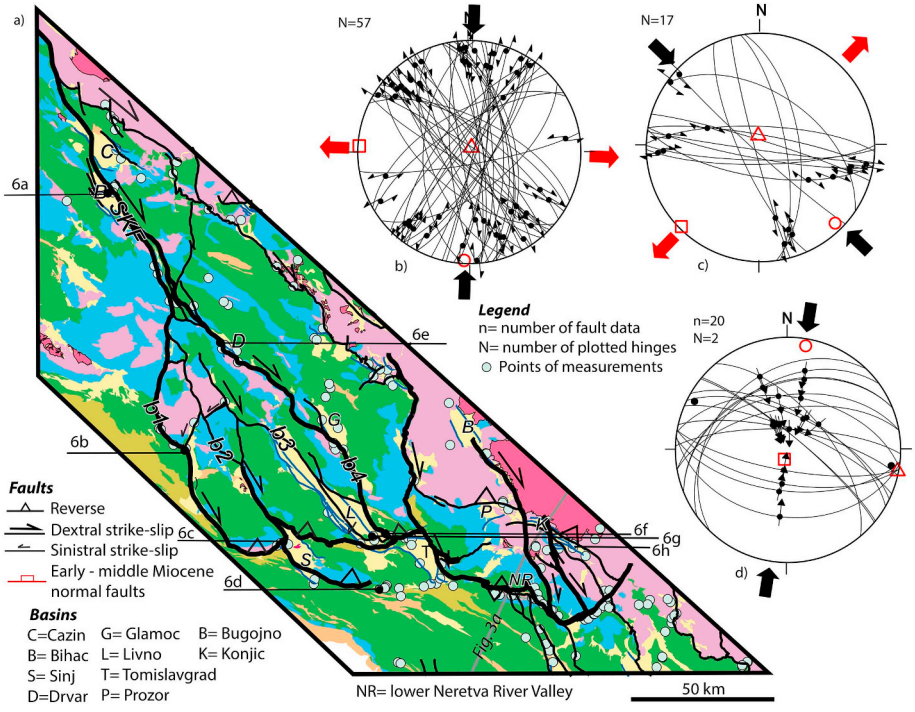

Fig. 5. Structural map and kinematic data for the area of Split-Karlovac and connecting fault system. Note that only structures active in the post- 9 Ma phase of deformation are displayed in the entire map and plotted on stereonets (Schmidt projection, lower hemisphere), together with the early-middle Miocene normal faults displayed in the area of the Miocene basins. In stereonets, lines with arrow symbols are projections of fault planes with kinematic sense of shear, while thick black dots are projections of fold hinges. a) Geological map with structures active during the post- 9 Ma phase of deformation. b1–4 are individual branches of the fault system. SKF = Split-Karlovac Fault (branch b1 of the fault system). Same conventions and legend as in Fig. 2. Location of the map is displayed in Fig. 2. b) Stereoplot showing NW-SE to NNW-SSE oriented dextral and their conjugate NNE-SSW to ENE-WSW oriented sinistral strike-slip faults. The calculated average paleostress solution shows N-S oriented compression and E-W oriented tension; c) Stereoplot showing WNW-ESE oriented dextral and NNW-SSE oriented sinistral strike-slip faults. The calculated average paleostress solution shows NW-SE oriented compression and NE-SW oriented tension; d) Stereoplot showing reverse faults and two sub-horizontal fold hinges, the calculated average paleostress solution shows N-S to NNE-SSW oriented compression.

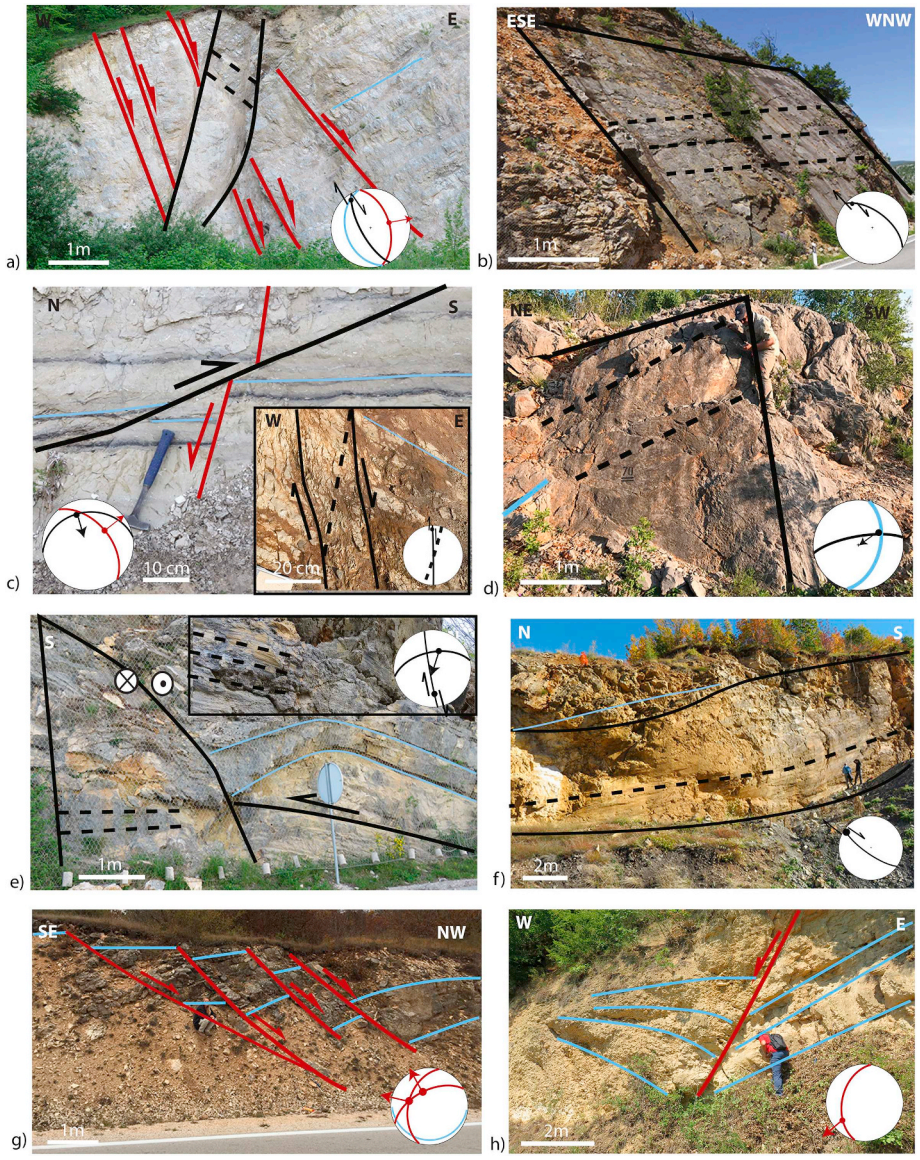

Fig. 6. Interpreted field photos illustrating structures and their kinematics in the area of the Split-Karlovac and connecting fault system (locations in Fig. 5a). Red lines: early–middle Miocene faults, black lines: post- 9 Ma faults, blue lines: bedding. a) One NW-SE oriented dextral strike-slip shear zone cross-cutting (E)NE-dipping normal faults in Jurassic limestones along the NE flank of the Bihac Basin; b) One large offset NW-SE oriented dextral strike-slip fault truncating Cretaceous limestone deposits along the Split-Karlovac Fault; c) One small-offset S-vergent reverse fault cross-cuts a NE-dipping normal fault, adjacent to a N-S oriented dextral strike-slip fault gauge zone with Riedel shears in lower Miocene lacustrine sediments of the Sinj Basin; d) One high-angle SW-vergent reverse-sinistral fault in Cretaceous limestones located in the footwall of a large-offset high-angle reverse fault; e) One NNW-SSE oriented dextral strike-slip fault cross-cuts a low-angle SSW-vergent reverse fault and drag folding in Jurassic limestones situated along the SW flank of the Drvar Basin. The upper right inset shows slickensides along the strike-slip fault plane; f) Large-offset NW–SE oriented dextral strike-slip shear zone truncating Miocene sediments and Cretaceous limestones in the SE part of the Livno Basin; g) One system of NW-dipping normal faults located in the Livno Basin; h) One NNE-SSW oriented normal fault associated with *syn*-depositional middle Miocene sedimentation in the Konjic Basin. The syn-kinematic wedge is filled with coarse conglomerates. (For interpretation of the references to colour in this figure legend, the reader is referred to the web version of this article.)

having the same kinematics in a narrow deformation zone. When multiple kinematics was observed in a fault or shear zone, the last kinematic sense of shear derived by superposition criteria was considered for the subsequent analysis, while older ones were compared with the kinematic history known from previous studies. Field measurements included brittle structures, such as faults with their kinematic sense of shear derived from slickensides, Riedels, or drag-folds, other types of folds, shear foliations and shear-bands. The regional mapping and kinematic observations have allowed the definition of a regional post-middle Miocene fault system that inverted the Miocene basins across the entire studied area (black faults in Figs. 2, 5, 7 and 9). In order to illustrate overprinting relationships and truncations, we also plotted Cretaceous-Paleogene faults and major units contacts defined by stratigraphic juxtaposition in the previous studies mentioned above. Although we have observed and described numerous partly *syn*-depositional normal faults in or outside the Miocene basins, their lower offset and subsequent truncations do not allow the definition of a fault system that can be regionally connected in our study. As a consequence, we can regionally interpret these faults only in the area of the Miocene basins. Furthermore, all measured normal faults indicate the same bi-modal N*E*-SW to NW-SE extension directions with major faults oriented NW-SE, as observed by previous studies (Fig. 2, Andrić et al., 2017; van Unen et al., 2019). Therefore, we focussed our regional interpretation to describe only the geometry and kinematics of the post- 9 Ma deformation event.

Our specific strain-based approach over the large study area and the observed deformation patterns are not suitable to invert the kinematic data to obtain well-constrained paleostress directions. This methodological limitation comes first from the fact that measurements in large offset fault zones are far from the Wallace-Bott criteria. Furthermore, rocks affected by deformation are highly anisotropic, such as often contacts between turbidites and limestones (re-)activated by faulting, and the measured large offset faults have a highly curved geometry where the observed kinematics suggests vertical axis rotations. Often reactivations and partitioning of deformation in large drag folds, restraining strike-slip bends, step-overs, wedge and tear faulting require a high-resolution data set that is beyond the regional scope of our study. Such limitations of the paleostress methodology are otherwise well-known (e.g., Célérier et al., 2012; De Vicente et al., 2009; Hippolyte et al., 2012; Jones and Tanner, 1995; Orife and Lisle, 2003; Sperner and Zweigel, 2010). While there is no standard paleostress methodology in such large offset faults mapping situations, we use our post- 9 Ma fault slip observations to derive average paleostress solutions at the scale of our focus areas that are consistent with the observed strain pattern (Simón, 2019). These solutions are not different tectonic events, as all are faults constrained by the same post- 9 Ma timing constraints. Such

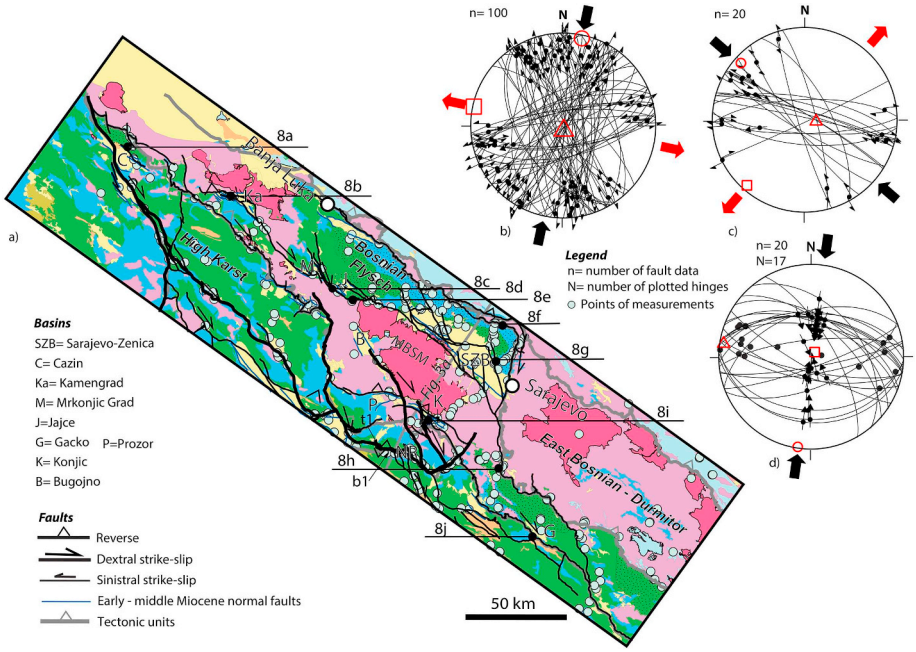

Fig. 7. Structural map and kinematic data for the Bosnian Flysch and connecting fault system. Note that only structures active in the post- 9 Ma phase of deformation are displayed in the entire map and plotted on stereonets (Schmidt projection, lower hemisphere), together with the early-middle Miocene normal faults displayed in the area of the Miocene basins. In stereonets, lines with arrow symbols are projections of fault planes with kinematic sense of shear, while thick black dots are projections of fold hinges. MBSM = Mid-Bosnian Schist Mountains, SZB = Sarajevo-Zenica Basin. a) Geological map with structures active during the post- 9 Ma phase of deformation. Same conventions and legend as in Fig. 2. Location of the map is displayed in Fig. 2. t1 and b1 are the thrust and backthrust discussed in the text and displayed also in Fig. 3a. b) Stereoplot showing NW-SE to N-S oriented dextral and their conjugate NNE-SSW to ENE-WSW oriented sinistral strike-slip faults. The calculated average paleostress solution shows NNE-SSW oriented compression and ESE-WNW oriented tension; c) Stereoplot showing WNW-ESE oriented dextral and NNW-SSE oriented sinistral strike-slip faults. The calculated average paleostress solution shows NW-SE oriented compression and NE-SW oriented tension; d) Stereoplot showing reverse faults with S- and N- sense of shear, and ~E-W oriented fold hinges. The calculated average paleostress solution shows NNE-SSW oriented compression.

solutions have been proved to be effective to derive tectonic significant constraints for deformation in places where complex strain and stress partitioning is observed (e.g., Matenco et al., 2007; van Gelder et al., 2015 among others). The paleostress solutions were obtained by a direct inversion method (Angelier, 1979; Angelier, 1984; Delvaux and Sperner, 2003), accounting for confidence criteria (Sperner and Zweigel, 2010) and allowing a slip tolerance of ± 26° (Lisle, 2013). We use these paleostress solutions (Figs. 5, 7 and 9b–d) mainly for a comparison with the present-day stress distribution, a procedure that allows the projection of the tectonic regime back in time (e.g., Lacombe, 2012). Displacements along the observed faults are used as independent constraints to correlate with the calculated average paleostress solutions, which interpreted to be part of the material response to imposed boundary conditions (Fig. 12a, b, Tikoff and Wojtal, 1999). The kinematic data are correlated with previous studies on GPS motions, seismicity and available focal mechanisms, crustal geophysics and regional geodynamic constraints in the Dinarides and at the larger-scale of the Adriatic continental micro-plate. We specifically use in interpretation a differentiation between strain (contraction-extension) and stress (compression-tension) nomenclatures.

We have calculated the total amount of deformation observed in the studied area by combining measurements of strike-slip offsets with a cross-section restoration. Strike-slip offsets were estimated using stratigraphic markers and the average pitch of the kinematic sense of shear along each individual faults. Understanding the geometry of deformation is aided by two kinematically-controlled cross-sections, whose trace was specifically chosen to avoid large out-of-plane strike-slip offsets and are parallel with average transport directions (Fig. 3a, b, van Unen, 2019). These two cross-sections are using the same surface kinematic and stratigraphic constraints and the same depth projection constraints in the onshore as described by van Unen et al. (2019). However, the sections were re-interpreted at depth by assuming a modified Moho geometry taken from the gravity inversion of Šumanovac (2010). The sections were prolonged in the Montenegro offshore by seismic interpretation (Fig. 3b) and by a less-constrained geological interpretation in the Croatian offshore (Fig. 3a), by accounting for the deformation observed along the ~ E-W oriented Middle Adriatic Ridge (Fig. 1, e.g., Scisciani and Calamita, 2009). Further details on the construction of these sections and alternative interpretations are available elsewhere (Bega, 2015; van Unen et al., 2019; van Unen et al., 2019). A first estimate of the amount of deformation observed in these cross-sections was obtained by measuring offsets and by simple flexural-slip unfolding the stratigraphy. Another estimate is available from a restoration of the previously interpreted onshore part of the Montenegro transect in Fig. 3b (van Unen et al., 2019). However, given also the re-interpretation of the cross-section, a new, better constrained restoration was performed at higher resolution on the external part of the Dinarides. The Montenegro transect (Fig. 3b) was quantitatively restored by using the KronosFlow™ software (IFPEN and BeicipFranlab, http://www.beicip.com/2d-kinematics-basin-modeling, Fig. 11), which allows preserving the lithostratigraphic character of each horizon and subdivision of cross-sections into different blocks with their own specific grid and dimensions. Faults are restored by using a moving least square method, which makes a global approximation of all available (unorganized) data points of the two sliding surfaces (both faults or horizons) and restores towards the region around the point for the best-fit reconstruction (Lancaster and Salkauskas, 1981). A flexural slip geometry method was used to restore extensional geometries, which unfolds objects around a straight line (e.g. fault) and preserves area, volume and line length (Dahlstrom, 1969). The restoration accounts for decompaction calculated between two deformation phases to adjust with sediment unloading (i.e. backstripping) by using standard porosity relationships for the lithological distribution in each tectonic unit (Fig. 4). Timing indicators, stratigraphic markers and their unfolding geometry were used, where available, to step-wide restore the section during each deformation step back in time until the Late Cretaceous.

4. Kinematic data along the Dinarides strike

The observed post-Paleogene structures are either normal faults that formed during the onset of the early-middle Miocene basin sedimentation or a combination between strike-slip connected with high angle reverse faults or thrusts that post-date (truncate) Miocene

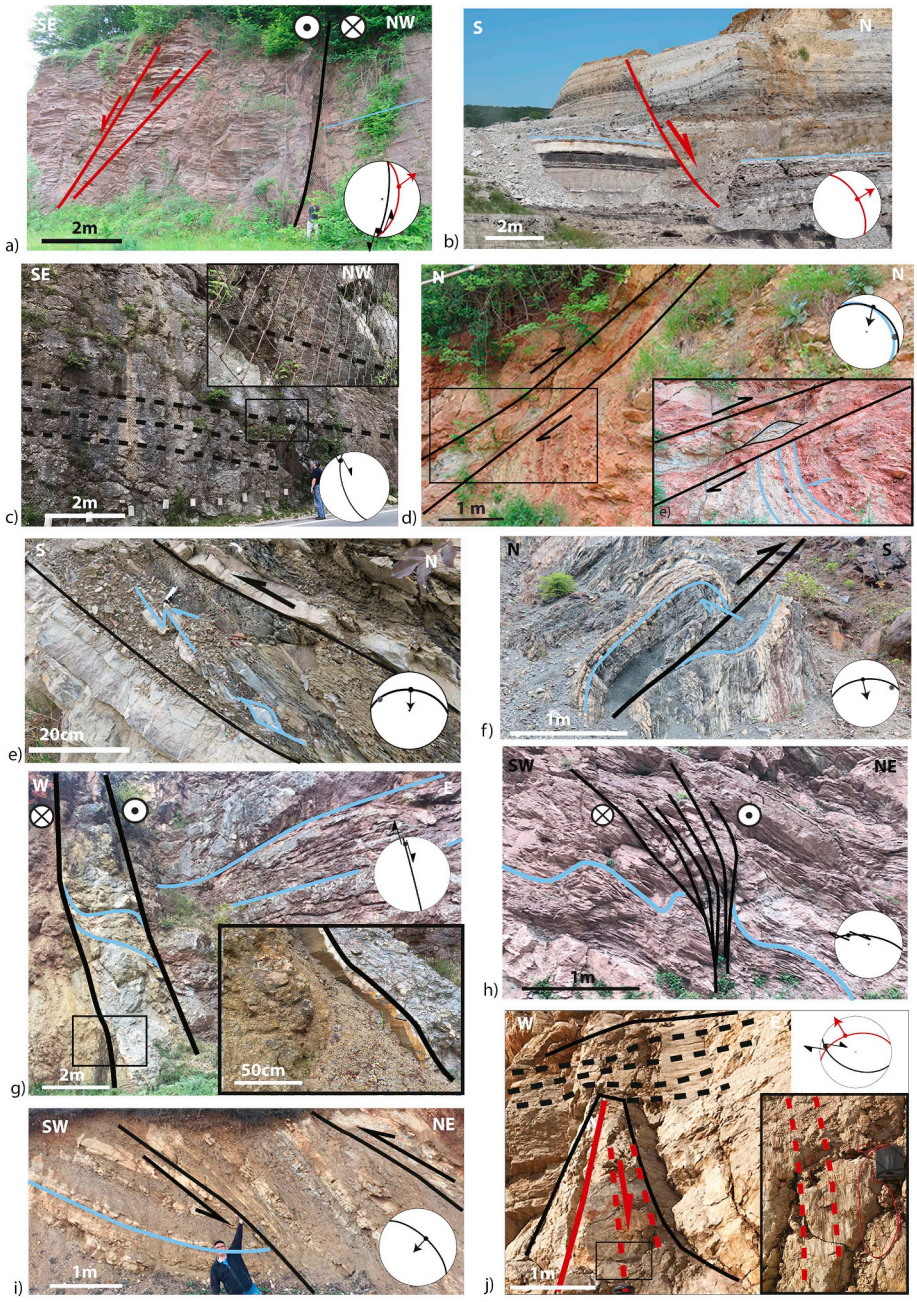

Fig. 8. Interpreted field photos illustrating structures and their kinematics in the area of the Bosnian Flysch and connecting fault system (locations in Fig. 7a). Red lines: early–middle Miocene faults, black lines: post- 9 Ma faults, blue lines: bedding. a) One NNE-SSW oriented sinistral strike-slip shear zone adjacent to NE-dipping normal faults truncating uppermost Cretaceous turbidites of the Ugar Flysch along the NE flank of the Cazin Basin; b) One large-offset (~15 m) NE-dipping normal fault truncating the Miocene sediments of the Kamengrad Basin; c) One NW-SE oriented dextral strike-slip fault truncating Cretaceous limestones, part of a larger system of similarly oriented dextral strike-slip faults that offsets with ~10 km the Jajce from Mrkonjic Grad basins; d) One S-vergent reverse shear-zone truncating Cretaceous limestones located south of the Jajce Basin. The bottom right inset shows brittle shear-bands and Riedel shears formed in the fault gouge foliation and drag-folding in the footwall; e) One S-vergent reverse shear-zone associated with brittle shear-bands and asymmetric folds with a WNW oriented hinge located in the Upper Jurassic turbidites of the Vranduk Flysch; f) One S-vergent reverse fault associated with drag folds with an E-W oriented hinge, located in the Upper Jurassic – lowermost Cretaceous ophiolitic mélange; g) One NNW–SSE oriented dextral strike-slip shear zone with kilometres-size offset truncating the uppermost Cretaceous turbidites of the Ugar Flysch. The bottom right inset shows thick slickensides inside the ~2 m thick fault gouge foliation; h) Transpressional flower structure made up of WNW-ESE oriented dextral strike-slip faults truncating the uppermost Cretaceous turbidites of the Ugar Flysch; i) High-angle SW-vergent reverse fault associated with drag folding truncating the lower – middle Miocene sediments of the Konjic Basin; j) WNW-ESE oriented dextral strike-slip fault cross-cutting a NW-dipping normal fault truncating Jurassic limestones at the contact with the Miocene sediments of the Gatsko Basin. The bottom right inset shows the dip slip slickensides of the normal fault. (For interpretation of the references to colour in this figure legend, the reader is referred to the web version of this article.)

sediments. These strike-slip and contractional structures are connected by forming an anastomosing system of faults that truncate most of the studied Dinarides area from the NW to the SE (Fig. 2). These structures may be grouped in three main areas based on the amplitude and character of deformation, i.e. the Split-Karlovac faults system, the Bosnian Flysch and connecting faults system, and the Budva unit and connecting faults system (Figs. 5, 7 and 9, respectively).

4.1. The Split-Karlovac faults system

In the NW part of our studied area, the Split-Karlovac faults system is composed of one main fault zone in the NW that gradually branches off SE-wards in four main dextral strike-slip faults (Fig. 5a). In outcrops, often larger offset WNW-ESE to N-S oriented dextral strike-slip faults are associated with smaller offset NNW-SSE to NE-SW oriented conjugate sinistral faults. In map scale, the large-offset dextral faults change their strike and connect to thrusts or high-angle reverse faults (Fig. 5a). This is observed in outcrops by numerous WNW-ESE to WSW-ENE oriented large offset thrusts and high-angle reverse faults associated with few similarly oriented (drag-) folds. All these faults truncate, reactivate or fold the lower-middle Miocene sediments and the pre-Miocene nappe structure (Fig. 5a). The large-offsets strike-slip faults and reverse faults can be often observed at the present-day basin margins (Fig. 5a), which suggests transpressive movements associated with uplift and exhumation.

In the NW part of the studied area, near the Cazin and Bihac basins, the Split-Karlovac deformation is focused on one main NNW-SSE oriented fault that is located at the western margin of the former and the eastern margin of the latter (Fig. 5a). In outcrops, NNW-SSE oriented dextral shear zones cross-cut inherited and similarly oriented normal faults that are observed, for instance in the Upper Jurassic limestones at the eastern margin of the Bihac Basin (Fig. 6a). The lower-middle Miocene sediments are truncated by similarly oriented normal faults that are tilted together with the bedding near the margins affected by

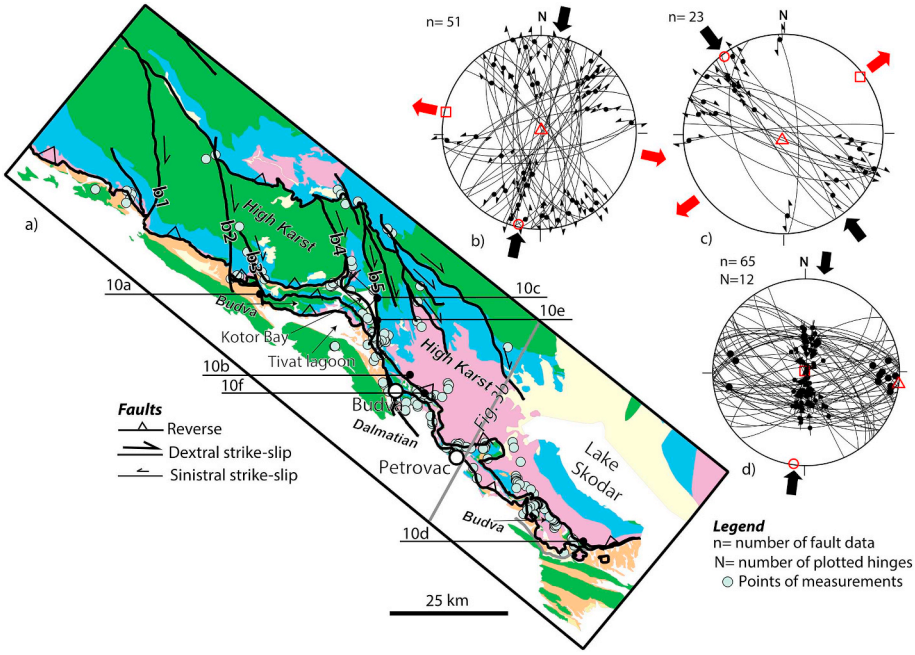

Fig. 9. Structural map and kinematic data for the Budva zone and connecting fault system. Note that only structures active in the post- 9 Ma phase of deformation are displayed in the entire map and plotted on stereonets (Schmidt projection, lower hemisphere), together with the early-middle Miocene normal faults displayed in the area of the Miocene basins. In stereonets, lines with arrow symbols are projections of fault planes with kinematic sense of shear, while thick black dots are projections of fold hinges. a) Geological map with structures active during the post- 9 Ma phase of deformation. Same conventions and legend as in Fig. 2. Location of the map is displayed in Fig. 2; b) Stereoplot showing NW-SE to N-S oriented dextral and their conjugate NNE-SSW to ENE-WSW oriented sinistral strike-slip faults. The calculated average paleostress solution shows NNE-SSW oriented compression and ESE-WNW oriented tension; c) Stereoplot showing WSW-ENE to WNW-ESE oriented dextral and NNW-SSE to N-S oriented sinistral strike-slip faults. The calculated average paleostress solution shows NW-SE oriented compression and NE-SW oriented tension; d) Stereoplot showing reverse faults with N and S sense of shear and ~E-W oriented fold hinges. The calculated average paleostress solution shows NNE-SSW oriented compression.

faulting. However, the Split-Karlovac Fault itself (fault b1 in Fig. 5a) and its vicinity is affected by significant diapirism of the Permo-Triassic salt and other evaporites (Šušnjara et al., 1992; Tišljar, 1992), which makes a clear discrimination of tectonic deformation rather difficult. This is rather obvious by the uplift of diapirs along the fault in its central part and in the Sinj Basin, east of the junction between two major branches of the system (Fig. 5a, see also de Leeuw et al., 2010).

From the north-west to the south and south-east, the strike-slip deformation is gradually being distributed along a wide area where the previously mapped Split-Karlovac Fault is the westward branch of our post- middle Miocene fault system (fault b1 in Fig. 5a). Along this fault trace, often dextral transpressive truncations and drag-folding of the steeply dipping (50–60°) Upper Eocene – Oligocene Promina beds is observed (Fig. 6b). In the same area, deformation is also associated with smaller-offset NE-SW oriented sinistral strike-slip faults and shear zones with foliated fault gouges that reach kilometres offsets (NE of point 6b in Fig. 5a). More to the SE, the Split-Karlovac Fault changes strike and become a high-angle reverse fault, where the Triassic clastics and limestones in the hanging-wall are thrusted over gradually tilted Promina and lower Miocene sediments of the Sinj Basin (SE termination of fault b1 in Fig. 5a).

To the NE, the second branch of the Split-Karlovac faults system (fault b2 in Fig. 5a) offsets the Promina beds and the Miocene sediments of the Sinj Basin near its SE-ward termination. This deformation is visible in the basin, for instance by centimetres to metres scale ENE-WSW oriented thrusts and N-S oriented strike-slip faults and shear zones that truncate centimetres- to metres-scale offsets normal faults (Fig. 6c). Truncation of stratigraphic markers shows that the offset of this second dextral strike-slip branch is in the order of a few kilometres in the north and increases to 10–15 km in the Sinj Basin (Fig. 5a). At its SE termination, the dextral strike-slip branch changes its strike and connects with a reverse fault. The offset of this reverse fault gradually decreases eastwards as observed by the stratigraphic duplication of Jurassic – Cretaceous limestones in its hanging-wall emplaced over Cretaceous – Oligocene limestones and clastics (including Promina beds) of the footwall (Fig. 5a). In outcrops, reverse faults often show a strike-slip component that changes from dextral in the west to sinistral in the east (Fig. 6d).

One other branch of the Split-Karlovac faults system (fault b4 in Fig. 5a) crosses the SW margin of the Drvar Basin and Glamoc Basin. In more details, NNW-SSE oriented dextral strike-slip faults changes their strike to or truncate ~S-vergent fault-bend folds affecting the Lower Cretaceous sediments and offsets Cretaceous limestones that border the western margin of the Drvar Basin (Fig. 6e). This dextral deformation also cross-cuts normal faults observed at the SW margin of the Glamoc Basin. To the SE, the third and fourth branches of the Split-Karlovac system (faults b3 and b4, Fig. 5a) truncate the SE part of the Livno Basin, where they form a large transpressive structure that splays and transfer offsets between dextral strike-slip to high angle reverse faults and transpressive structures. In this area, a 7–10 m thick shear zone made up by a foliated fault gouge can be observed, which has a clear NW-SE oriented dextral strike-slip character (Fig. 6f). The foliation is made up of fault gouge material that contains remnants of sheared Cretaceous limestones and Miocene lacustrine marls. This shearing also truncates the system of domino-tilted normal faults observed in the Miocene sediments of the same basin (Fig. 6g), while forming large drag-folds by tilting these strata to sub-vertical positions. The deformation associated with the overall NNW-SSE oriented transpressive structures at the SE margins of the Livno and Tomislavgrad basins are connected by an E-W oriented system of reverse faults associated with large drag-folding of the Cretaceous – Oligocene carbonates and clastic sediments in their footwalls (Fig. 5a). In fact, it is likely that Livno and Tomislavgrad formed as one basin during the Miocene extension and were separated by a subsequent uplift associated with this connected transpressive-reverse faults system (see also de Leeuw et al., 2011). Further to the SE (Fig. 5a), the dextral fault at the eastern margin of the Tomislavgrad Basin changes again its strike and is connected to a system of N- and S- vergent high angle reverse faults that are furthermore connected with the large offset fault system of the Neretva Valley described below.

The paleostress analysis of all post- 9 Ma kinematics of faults measured in the field has resulted in three average solutions. Strike-slip kinematics measured along NW-SE oriented dextral and NNE-SSW sinistral fault segments define a strike-slip stress field with a N-S oriented compression (Fig. 5b). Strike-slip kinematics measured along WNW-ESE oriented dextral and NNW-SSE sinistral fault segments define a strike-slip stress field with a NW-SE oriented compression direction (Fig. 5c). Fault kinematics measured along WNW-ESE to W-E oriented reverse faults define a N-S to NNE-SSW oriented compressional stress field (Fig. 5d).

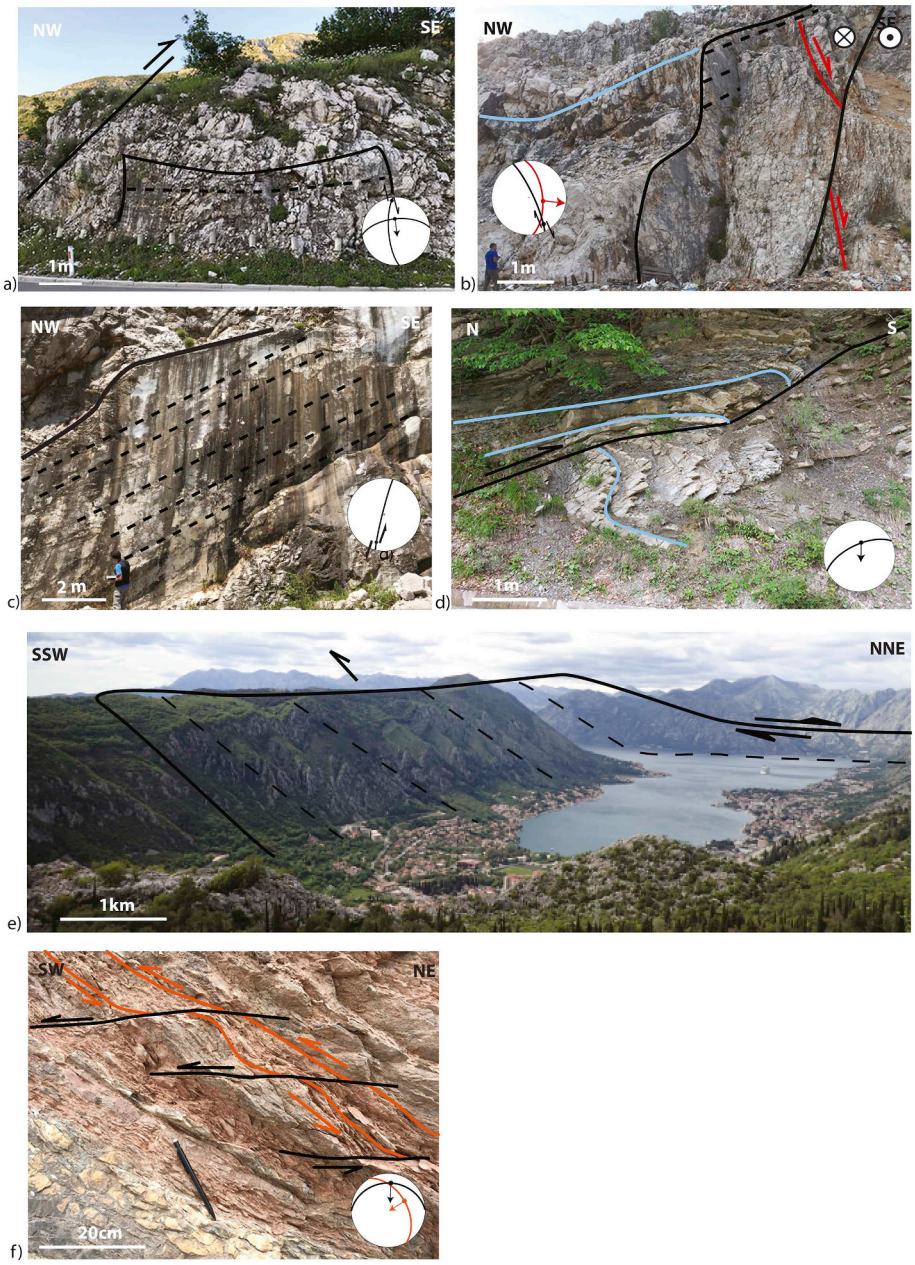

Fig. 10. Interpreted field photos illustrating structures and their kinematics in the area of the Budva unit and connecting fault system (locations in Fig. 9a). Red lines: early–middle Miocene faults, black lines: post- 9 Ma faults, blue lines: bedding. a) One NNW-SSE oriented dextral strike-slip fault and one high-angle S-vergent reverse fault truncating Cretaceous limestones, part of a larger shear zone made up by NNW-SSE oriented dextral strike-slip faults separating the Budva from Dalmatian units; b) One NW–SE oriented dextral strike-slip faults cross-cutting an ESE-dipping normal fault in Triassic carbonates of the High Karst unit. c) One large offset NNE-SSW oriented sinistral strike-slip fault truncating Cretaceous limestones of the High-Karst unit; d) One S-vergent reverse fault associated with drag folding deforming Eocene turbidites of the Budva unit; e) Large-scale overview of the Kotor Bay illustrating the transfer from dextral strike-slip faulting in the NNW- to S-ward thrusting to the SSE; f) Typical cross-cutting relationship between the two thrusting events observed in the Budva unit. Cataclastic shear bands with top SW sense of shear are cross-cut by more brittle shear with top-S sense of shear. (For interpretation of the references to colour in this figure legend, the reader is referred to the web version of this article.)

4.2. The Bosnian Flysch and connecting faults system

The second group of large-offset faults cross-cutting Miocene basins and the pre-Miocene orogenic structure are observed along a wide zone combining the southern margin of the East Bosnian – Durmitor unit, the Bosnian Flysch and the southern margin of the Mid-Bosnian Schist Mountains, where large-offset dextral faults change their strike and connect again to thrusts or high-angle reverse faults (Fig. 7a). The reverse faults can often be associated with drag and upright folds with ~E-W to WNW-ESE oriented hinges. All these structures deform or truncate the lower-middle Miocene sediments and the genetically associated normal faults in the Kamengrad, Jajce, Mrkonjic Grad, Sarajevo-Zenica and Konjic basins and the pre-Miocene nappe structure located along their flanks (Figs. 3a and 7a). Wide shear zones or areas with high-density faults with similar kinematics are generally dextral transpressive or high-angle reverse verging southwards, which suggests significant exhumation of the basins and their flanks (Figs. 3a and 7a).

In the NW, normal faults are often cross-cut or observed in the vicinity of strike-slip faults (Fig. 8a). Normal faults with similar orientations are furthermore observed in the lower part of the lower-middle Miocene sediments of the Kamengrad Basin (Fig. 8b), which are covered or absent in the upper basin stratigraphy.

A NNW-SSE oriented dextral strike-slip shear zone offsets the Miocene basin fills of the Mrkonjic Grad and Jajce Basins (Fig. 7a). This shear zone is visible in both the Miocene sediments and the Lower Cretaceous limestones situated along their flank, where it forms a dense network of large fault planes with clear slickensides (Fig. 8c) or shear zones with fault gouge foliations. To the SE, this fault zone changes gradually its strike to NW-SE and WNW-ESE, and is connected with an E-W oriented shear zone with reverse, sometimes oblique offset and S-ward vergence. In outcrops, this shear zone is observed as an up to 4 m thick foliated fault gouge that contains numerous brittle S—C and C-C′ shear-bands or Riedel structures (Fig. 8d). This shear zone drags and folds the strata or other foliated fault-gouge material in its footwall.

The Bosnian Flysch zone flanking the Sarajevo-Zenica Basin (Fig. 7a) retains a large amount of deformation that recorded both the pre-Miocene orogenic evolution, the Miocene extension and the subsequent shortening affecting the basin and its flanks (see also van Unen

et al., 2019). The latter structures are made up by metres-thick dextral strike-slip shear zones, high-angle reverse faults and thrusts with top-S sense of shear, layer parallel shearing and E-W oriented folds. For instance, often layer-parallel top-S shearing affects the finer members of the turbidite beds, observed by brittle shear bands and asymmetric folds (Fig. 3a and 8e). The contact zone between the East – Bosnian Durmitor and Bosnian Flysch units is often re-activated with a top-S sense of shear along high-angle reverse faults associated with metres scale drag-folds (Fig. 8f).

At the eastern margin of the Sarajevo-Zenica Basin, a NNW-SSE to N-S oriented dextral strike-slip shear zone, made up by several branches, cross-cuts both the Miocene basin sediments and the adjacent uppermost Cretaceous turbidites (Fig. 8g). These branches are often observed by metres-thick foliated fault gouges with clear slickensides, associated with brittle shear bands and Riedel shears. South of the Sarajevo-Zenica Basin, the eastern termination of the East Bosnian – Durmitor unit is most likely a large offset dextral fault that gradually changes strike and connects to an E-W oriented high-angle reverse fault (Fig. 7a). The gradual change is characterized by the formation of NW-SE to WNW-ESE oriented dextral transpressive and positive flower structures, observed in the uppermost Cretaceous calci-turbidites of the Bosnian Flysch (Fig. 8h).

South of the Mid-Bosnian Schists Mountains, one other transpressional strike-slip system can be observed in the southern part of the Bugojno Basin, that more to the south cross-cuts and offsets dextrally the Konjic Basin to the ESE from the Prozor Basin to the WNW (Fig. 7a). Large-offset (tens of metres) normal faults are often associated with *syn*-depositional early-middle Miocene sedimentation. For instance, the early-middle Miocene sediments of the Konjic Basin were deposited during the formation of numerous up to 30 m offset normal faults, which are often associated with the deposition of coarse conglomerates in the syn-kinematic wedge (Fig. 6h). In this basin, normal faults and Miocene sediments are truncated by 3 to 4 subsequent major dextral shear zones associated with transpressional or high-angle reverse faults. For example, a NW-SE oriented reverse shear zone crosscuts the centre of the basin and is associated with drag folding and tens of metres spaced fault branches (Fig. 8i), locally associated with metres-thick fault gouge foliations. Further to the SE, the continuation of this fault system is less clear in map view (Fig. 7a), but outcrops show numerous strike-slip faults, either WNW-ESE to NNW-SSE dextral or NNW-SSE to NNE-SSW sinistral that truncate often pre-existing normal faults. For instance, the Jurassic limestones and clastic sediments located on the SW flank of Gatsko Basin (Fig. 7a) show ENE-WSW oriented normal faults that are truncated by WNW-ESE oriented dextral strike-slip faults (Fig. 8j).

The paleostress analysis of all post- 9 Ma kinematics of faults measured in the field has resulted again in three average solutions. Strike-slip kinematics measured along NW-SE to N-S oriented dextral and roughly NE-SW sinistral fault segments define a strike-slip stress field with a NNE-SSW oriented compression (Fig. 7b). Strike-slip kinematics measured along WNW-ESE oriented dextral and NNW-SSE sinistral fault segments define a strike-slip stress field with a NW-SE oriented compression (Fig. 7c). Fault kinematics measured along WNW-ESE to WSW-ENE thrusts and high-angle reverse faults define a roughly NNE-SSW oriented compressional stress field (Fig. 7d).

4.3. The Budva unit and connecting faults system

Similar to the Bosnian Flysch zone, the Budva unit of Montenegro was intensively deformed during both the pre-Miocene orogenic evolution and the Neogene extension followed by shortening (van Unen et al., 2019). The most recent episodes of deformation include numerous normal faults observed in the Budva and neighbouring units that truncate sediments as young as the Eocene-Oligocene and, therefore, are considered to be Miocene in age by correlation with the syn-depositional normal faults found in the Dinarides Lake System basins. These normal faults are inverted or subsequently truncated by a complex system of strike-slip, transpressional, high-angle reverse and thrust faults. In outcrops, a dense network of WNW-ESE to N-S dextral strike-slip faults is associated with less frequent NNW-SSE to ENE-WSW oriented sinistral strike-slip faults (Fig. 9b, c). However, differently from previous areas, a significantly higher number of E-W to NW-SE oriented thrusts and high-angle reverse faults have been measured in the Budva unit, which are more numerous at or near southward thrusted (sub-) units contacts and are often associated with drag and upright folds with ~E-W to WNW-ESE oriented hinges (Fig. 9d). In map scale, these thrusts are connected with NNW-SSE oriented dextral strike-slip faults (Fig. 9a).

NW of the Kotor Bay area, three dextral strike-slip faults (b1, b2 and b3, respectively, in Fig. 9a) are connected with the frontal thrust over the Dalmatian unit, while the latter fault (b3) makes the NW-ward termination along strike of the Budva unit in Montenegro. Numerous strike-slip faults have been observed in outcrops, typically by large fault planes with thick slickensides affecting the Mesozoic limestones, locally associated with top-S high-angle reverse faults (Fig. 10a). More to the SE, another NNW-SSE oriented dextral shear zones and is connected with the Budva thrusting along the eastern margins of the Kotor Bay and Tivat lagoon (branch b5 in Fig. 9a). This shear zone is observed by dextral zones of fault gauge foliations or dextral faults truncating earlier normal faults (Fig. 10b) associated locally with NN*E*-SSW oriented sinistral strike-slip faults (Fig. 10c).

Our field data are similar with previous studies that indicate three types of high-angle reverse and thrust faults observed in outcrops in the external High Karst – Budva – Dalmatian areas (Fig. 9a, van Unen et al., 2019). The NW-SE oriented High Karst over Budva and Budva over Dalmatian units contacts formed initially during the top-SW Eocene-Oligocene nappe stacking. These contacts as well as smaller-offsets thrusts composing the Budva sub-units geometry have been reactivated by a later deformation episode that created reverse faults with top-S sense of shear (Fig. 9d). In the field, the latter set is observed truncating the post-Eocene normal faults. Typical deformations in outcrops are observed for instance by high-angle reverse faults truncating Middle Triassic deep-water limestones or by reactivating the low-angle High Karst – Budva contact observed by the oblique thrusting of Triassic limestones over Eocene clastic turbidites (Fig. 10d). At major thrust contacts, cataclastic shear zones are associated with a large number of isoclinal-, upright-, drag- and asymmetric- folds with E-W to WNW-ESE oriented hinges (Fig. 9d). The superposition between the initial Eocene-Oligocene nappe stacking and the subsequent thrusting event can be often observed in shear zones where top-SW cataclastic shear bands are truncated by top-S brittle faults (Fig. 10f).

The two types of major structures, NW-SE to N-S oriented dextral faults and top-S ESE-WNW to NW-SE oriented high-angle reverse faults or thrusts gradually change their strike and connect with each other in the footwall of the High-Karst thrusting (Fig. 9a). The connection is done in such a way that the map-scale faults displace the High-Karst unit, the Budva unit and locally the Eocene-Oligocene clastic sediments of the Dalmatian located at the contact with the Budva unit. However, these map-scale dextral strike-slip faults do not displace the Cretaceous limestones of the Dalmatian unit. The connection between dextral strike-slip and thrusts can be observed, for instance, in the Kotor Bay, where a NNW-SSE oriented dextral strike-slip fault (b4 in Fig. 9a) connects with the High-Karst thrust (Fig. 10e), while the similarly oriented, larger offset dextral strike-slip branch located a few kilometres more to the east connects with the Budva thrust (b5 in Fig. 9a). At regional scale, the amount of southward thrusting of the High Karst unit increases towards the SE, as shown by the observed increase of internal deformation in the Budva unit and by an increase in exhumation leading to the gradual exposure of older (Triassic) rocks SE-wards in the High Karst unit (Fig. 9a).

The paleostress analysis of all post- Paleogene strike-slip and reverse faults kinematics measured in the field shows the same three average

solutions as in the previous areas, but with differently distributed number of faults. Strike-slip kinematics measured along NW-SE to N-S oriented dextral and roughly NE-SW sinistral fault segments define a strike-slip stress field with a NNE-SSW oriented compression (Fig. 9b). Strike-slip kinematics measured along WNW-ESE oriented dextral and NNW-SSE sinistral fault segments define a strike-slip stress field with a NW-SE oriented compression (Fig. 9c). Fault kinematics measured along the numerous WNW-ESE to WSW-ENE thrusts and high-angle reverse faults define a roughly NNE-SSW oriented compressional stress field (Fig. 9d).

4.4. Post- 9 Ma deformation estimates and a quantitative restoration of deformation history

All these observations in the three main key areas show that the post- 9 Ma faults form in map view a large anastomosing system that spans from the Cazin Basin in the NW to the connection with the Albanides in the SE (Figs. 1 and 2). These observations show that in all map-scale situations WNW-ESE to N-S oriented dextral faults are connected with E-W to WNW-ESE oriented reverse faults and thrusts. In fact, these are two segments of the same curved fault that change kinematics along these differently oriented segments, as shown by following the main shear zone kinematics. The dextral offset along these faults can be calculated by using stratigraphic markers and the average pitch of the measured shear-sense, while the reverse offset can be estimated in cross-sections or more precisely calculated in restorations. Given the inherited tectonic history, such estimates have a higher reliability in places where Miocene sediments are present as stratigraphic markers. Beyond simple estimates, a significant variability of offsets of strike-slip or thrust faults is also observed along strike, as further explained.

Estimates show that large dextral faults have variable maximum offsets between hundreds of metres and 25 km. For example, the offset of individual branches of the Split-Karlovac faults and the fault at the eastern margin of the Tomislavgrad basin system measured in their southern part in Miocene or Eocene-Oligocene stratigraphic markers is in the order of 10–15 km, while close to their northern termination the offset decreases to hundreds of metres to kilometres at the level of Triassic markers (Fig. 5a). A NNW-SSE oriented dextral strike-slip shear zone offsets with 10 km the lower stratigraphic infill of the Mrkonjic Grad Basin and Jajce Basin (Fig. 7a). A NNW-SSE oriented dextral strike-slip fault offsets the Miocene fill of the Kamengrad Basin with around 7 km (Fig. 7a). The total cumulated offset of the dextral system that displaces the lower stratigraphic infill of the Miocene Konjic Basin is in the order of 10–15 km (Fig. 7a). A thrust-backthrust system in the Neretva Valley (t1 and b1 in Figs. 3a and 7a) is displaced by a dextral system with 25 km at the level of Triassic markers. The total offset recorded by the dextral strike-slip system located at the eastern termination of the Sarajevo-Zenica Basin is rather difficult to calculate, but by accounting for the change in strike of the Bosnian Flysch and overlying East Bosnian – Durmitor unit (Figs. 1 and 7a, the Sarajevo "sigmoid" of Dimitrijević, 1997) this offset should be in the order of 15–20 km. In the Budva zone dextral faults gradually increase their offset from a few kilometres in the NW to more than 10 km in the SE (Fig. 9a, b). The three large scale dextral strike-slip faults located NW of the Kotor Bay area have map offsets in the order of 3, 5 and 7 km by using Eocene-Oligocene markers (b1, b2 and b3, respectively, in Fig. 9a). More to the SE, the same markers indicate that the NNW-SSE oriented dextral shear zones that displaces both the High-Karst and Budva contacts along the eastern margins of the Kotor Bay and Tivat lagoon has an offset in the order of 18 km (branch b5 in Fig. 9a). All other dextral faults in the three key areas were similarly estimated to have between 200 m and 10 km offsets.

Shortening estimates along thrusts can be obtained by the restoration of kinematically controlled cross-sections constructed along the sense of shear in time steps, performed for the Montenegro transect (Fig. 3b). Given kinematic observations linking strike-slip with reverse faulting along the trace of the same fault that changes strike, the step-wise restoration assumes that the offset measured along dextral faults is transferred to the post- 9 Ma top S-ward shortening along connected thrusts in the High-Karst and Budva zone (Fig. 9a). The restoration of these two thrusting events is constrained by stratigraphic markers offshore. The East Bosnian – Durmitor thrusting in the northern part of the profile is Late Cretaceous in age, the same contact being reactivated by the early-middle Miocene extension (EBD in Fig. 3b, Schmid et al., 2008; van Unen et al., 2019). In the absence of clear stratigraphic markers, the pre-Karst 10 km total thrusting offset (PK in Fig. 3b) was arbitrarily divided in equal 5 km offsets for the last two phases of Eocene-Oligocene and post- 9 Ma thrusting.

The kinematic restoration (Fig. 11) shows a total of 150 km of shortening for the Montenegro transect, distributed as 53 km post-9 Ma, 85 km Eocene-Oligocene and 22 km Late Cretaceous, together with 10 km of early-middle Miocene extension. The Eocene-Oligocene, Late Cretaceous and cumulative total shortening are minimum estimates given available depth projection constraints. In more details, most of the post- 9 Ma thrusting is focussed at the High-Karst over Budva (17 km), internal Budva (15 km) and Budva over Dalmatian (13 km) contacts, while the Eocene-Oligocene shortening is focussed at the Dalmatian over Adriatic (45 km) and Budva over Dalmatian (17 km) contacts.

Similar estimates can also be obtained for the Bosnia and Herzegovina – Croatia transect (Fig. 3a), although a good step-wise reconstruction cannot be achieved due to the less clear separation between Eocene-Oligocene and post- 9 Ma amounts of shortening in the offshore, and due to the absence of post-Paleozoic sediments in the Mid-Bosnian Schist Mountains. However, a rough estimate by measuring fault offsets and simple unfolding of the cross-section shows a total amount of shortening in the order of minimum ~140 km. Among this 50–70 km must have formed in post- 9 Ma times, combined with ~ 25 km of early-middle Miocene extension. The thick-skinned thrusting in the offshore is related to the Middle Adriatic Ridge, which is a set of offshore Adriatic E-W oriented structures with relatively low offsets that are interpreted to be formed in two stages, during Paleogene-Miocene and late Pliocene – Quaternary times (Fig. 1, e.g., Scisciani and Calamita, 2009 and references therein). The induced Paleogene-Miocene offset is very low and has a poor stratigraphic control, while the orientation of these structures is fairly compatible with the post- 9 Ma deformation observed onshore.

5. Understanding the kinematic data at regional scale

When connecting kinematic observations across all studied areas, it is rather clear that the pre-Miocene nappe system together with the Miocene basins of the Dinarides Lake System are affected by two deformation events along the strike of the entire Dinarides, which post-date the main period of orogenic structuration that ended during Paleogene times.

The first deformation event is characterized by *syn*-depositional normal faults that are genetically associated with the onset of early-middle Miocene sedimentation. Such normal faults were observed in all studied basins (Kamengrad, Drvar, Glamoc, Sinj, Livno, Tomislavgrad, Mrkonjic Grad, Jajce, Sarajevo-Zenica, Konjic, Gatsko, e.g., Fig. 6h) and provide critical timing constraints for the superposition of deformation. Although not targeted specifically by our kinematic analysis, we have observed that larger offset normal faults indicate roughly N*E*-SW extension, while smaller offsets normal faults show NW-SE oriented extension, which is agreement with what has been previously observed in other Dinarides basins of Bosnia and Herzegovina, Croatia, and Slovenia (e.g., Andrić et al., 2017; van Unen et al., 2019; Žibret and Vrabec, 2016). Therefore, we agree with these previous studies that a period of early-middle Miocene extension has affected all external areas of the Dinarides.

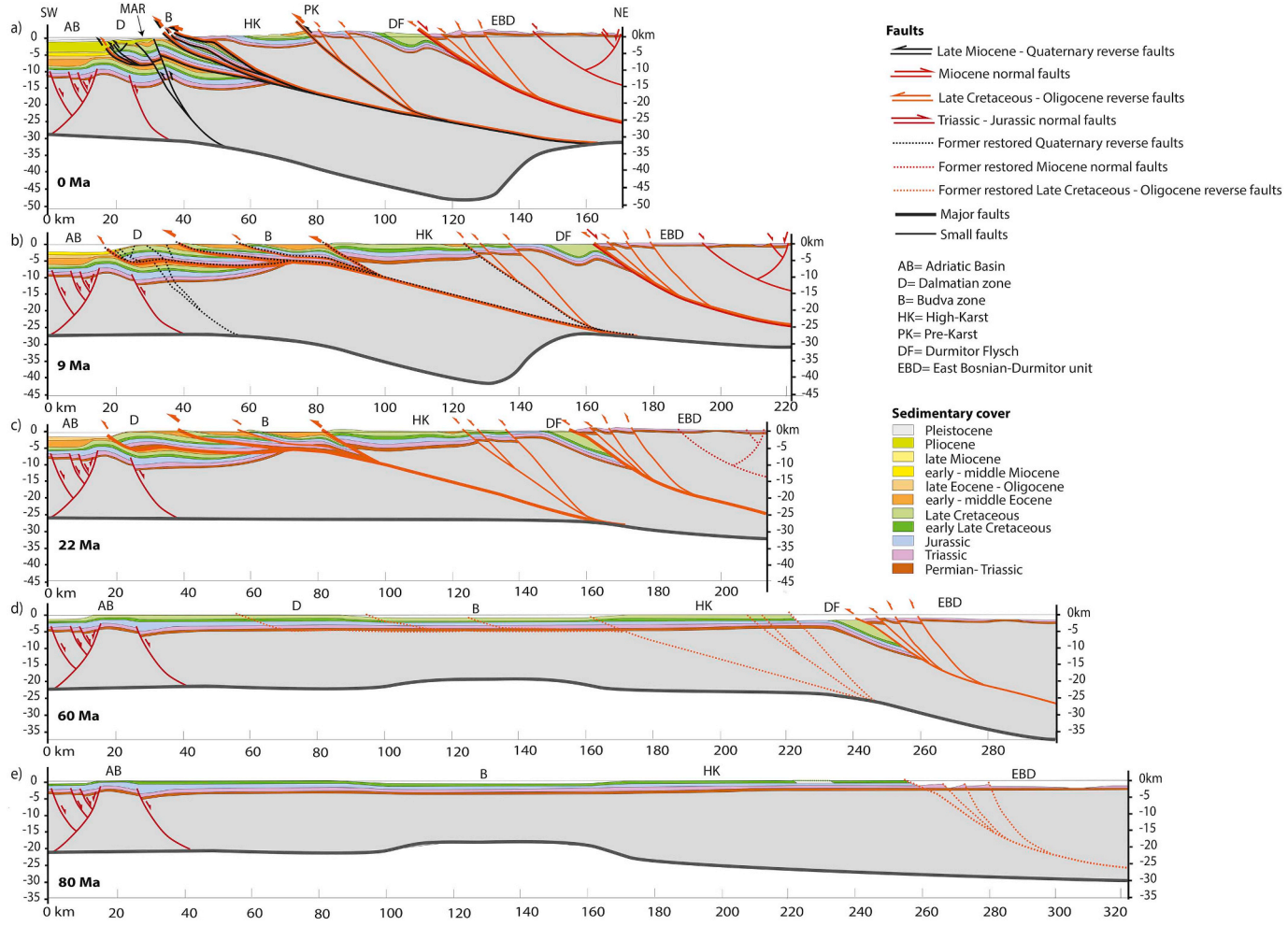

Fig. 11. Kinematic and quantitative step-wise restoration of the Montenegro cross-section displayed in Fig. 3b by using the KronosFlow™ software (location is displayed in Figs. 1 and 2). All observed strike-slip faults are located outside the trace of the profile. The step-wise constraints of the restoration are discussed in the text. AB = South Adriatic Basin; D = Dalmatian zone; B = Budva zone; HK = High-Karst unit; PK = Per-Karst; EBD = East Bosnian-Durmitor unit; DF = Durmitor Flysch; MAR = Middle Adriatic Ridge. a) the present-day transect, slightly simplified from Fig. 3b; b) restoration of the post- 9 Ma deformation; c) restoration of the early-middle Miocene extension; d) restoration of the Eocene-Oligocene thrusting; e) restoration of the latest Cretaceous thrusting.

More importantly, our study has defined for the first time the kinematics and geometry of a second major deformation event that took place after 9 Ma and post-dated the sedimentation in the early – middle Miocene basins by inverting, truncating or otherwise deforming their entire infill. Strike-slip faults observed in outcrops, can be correlated with large offset (hundreds of metres to 25 km) WNW-ESE to N-S oriented dextral offsets, while NNW-SSE to ENE-WSW oriented sinistral strike-slip faults have significantly smaller offsets less than few hundred metres. In almost all situations, these fault segments were already observed previously and drawn on available geological maps. However, only the Split-Karlovac Fault has been previously interpreted as a dextral strike-slip structure (branch b1 in our Split-Karlovac system, Figs. 1 and 5a, e.g., Chorowicz, 2016; Ustaszewski et al., 2008).

The timing of the Split-Karlovac Fault is the least controlled in our study, owing to the association of deformation with diapirs made up of salt and other evaporites and poor Miocene outcrops along this fault (Fig. 5a). Along this fault segment, the mapped deformation affected both the upper Eocene – Oligocene Promina beds and the locally overlying lower-middle Miocene sediments. However, the degree of deformation is significantly different: while the Promina beds are clearly truncated by this fault and often tilted to sub-vertical positions by drag-folds, Miocene sediments appear to be less deformed, while their degree of tilting is significantly lower, generally 20–40°. While it is possible that this difference in the degree of deformation observed is an effect of differential movements against the fault plane during the post-9 Ma deformation event, it is also possible that the Split-Karlovac Fault has been initiated earlier, during the late Eocene – Oligocene deposition of the Promina beds, and deformation continued later, after 9 Ma. This earlier initiation is inferred by the observation of thick Promina deposition limited to the west and south of the Split-Karlovac Fault, while to the east and north such deposition is fairly limited (Fig. 2). However, erosional removal during subsequent transpressional (re-)activation along the Split-Karlovac Fault could have played a significant role in this present-day thickness variability.

All other branches of the strike-slip and reverse faults system are much less or not affected by diapirism. These branches truncate both the Promina beds and Miocene sediments, whenever present, and must have been (re-)activated with a large offset after 9 Ma. There is just one kinematic study published so far documenting a late Eocene-Oligocene deformation in the Sarajevo-Zenica Basin, which is characterized by N*E*-SW shortening (Andrić et al., 2017). Such a shortening direction is fairly incompatible with the activation of the NW-SE to NNW-SSE dextral strike-slip along the Split-Karlovac Fault and, therefore, the first hypothesis of significant (re-)activation after 9 Ma seems more likely. Therefore, we conclude that most of the strike-slip connected with reverse faults along the entire Split-Karlovac system must post-date 9 Ma and has possibly reactivated an inherited Paleogene thrust.

The cumulative post- 9 Ma dextral strike-slip and reverse faulting

appears to be similar in the order of 50–70 km in the studied orogenic transects. However, this amount is distributed differently along the Dinarides orogenic strike (Fig. 2). In the NW, the largest amount of displacement of ~50 km is retained by the branches of the Split- Karlovac system, while more internal areas (around Kamengrad Basin) have lower amounts of total deformation (~10–15 km). In the centre, the largest amount of deformation is taken up by the Sarajevo – Zenica Basin together with its eastern Bosnian Flysch and East Bosnian – Durmitor units' change in strike along the Sarajevo "sigmoid" (~40 km), while deformation southwards in the Konjic Basin and Neretva valley has lower values (~30 km). In the SE, the largest amount of deformation is taken up by the external High-Karst and Budva units and its NNW-SSE connected dextral strike-slip faults 45 km), the remainder of 10 km being distributed between more internal units and more external offshore thrusting and internal deformation of the Dalmatian unit (Fig. 11).

The overall deformation shows a gradual transfer of dextral strike-slip, transpression and shortening from the internal Dinarides in the NW to the external Dinarides in the SE. The total amount of cumulative displacements across the entire system is difficult to estimate due to the unclear amount of offset transfer between individual structures, but the total amount of offset measured along all faults, by taking either the strike-slip or the reverse offset in the case of connected curved faults, is in the order of 150–200 km.

One special note is required for what has been previously described as the Pre-Karst thrusted unit of the Dinarides (Figs. 1 and 2). This unit has been introduced originally as a transitional paleogeographic realm between the Middle Triassic – Paleocene shallow-water carbonates of the external Dinarides and a more internal tectonostratigraphic unit characterized by deep water Upper Jurassic – Cretaceous turbidites (i.e. "flysch", see also Aubouin et al., 1970). In subsequent studies, the Paleozoic basement and the overlying continental to shallow-water Triassic to Cretaceous cover together with the overlying deformed Bosnian Flysch has been often grouped in an individual thrusted unit in the pre-Miocene Dinarides nappe stack (e.g., Schmid et al., 2008 and references therein). Our field observations show that in most areas of Bosnia north-west of the Neretva River (NW of NR in Fig. 7a), the contact between the Pre-Karst and High-Karst units never retains a typical SW-ward thrusting kinematics of the pre-Miocene deformation (the Dinaric vergence of Schmid et al., 2008; Tari, 2002). We observed that this fault is either a NW-SE to WNW-ESE oriented dextral strike-slip fault or an E-W oriented thrust with top S- to SSW-wards kinematics, or even a normal fault (Fig. 2). In other situations, the fault simply does not exist, the interpreted unit contact being a map interpretation connecting two faults with different kinematics (such as two post- 9 Ma strike-slip faults or a Dinaric thrust with a post- 9 Ma strike-slip fault, Fig. 2). It is rather clear that the segments of this contact with large offset are part of the post- 9 Ma dextral strike-slip and reverse faults system. Therefore, we suggest abandoning the term "Pre-Karst" as a pre-Miocene thrusted unit of the Dinarides.

6. Mechanics of deformation

The post- 9 Ma deformation observed in outcrops and map scale demonstrate in all areas that large offset WNW-ESE to N-S oriented dextral strike-slip faults transfer gradually their displacements to E-W to WNW-ESE oriented thrusts and high-angle reverse faults. Such structures are observed throughout the entire studied area (Fig. 2). Furthermore, a number of situations show that offset is transferred gradually from one curved strike-slip to reverse fault to another such fault in transfer zones. Such transfer zones are observed when the post – 9 Ma faults overlap along their strike with a general en-echelon geometry (Figs. 2 and 12). Whenever the deformation is taken up by one large offset dextral strike-slip fault, this offsets remains roughly constant along its strike outside transfer zones (outside grey areas in Fig. 12a). In the transfer zone, the offset of reverse faults is maximum near the dextral fault, while decreasing gradually at farther distance, often until complete disappearance. The gradual decrease in offset along these reverse faults is an effect of transferring the deformation to the next curved fault made up by another dextral and reverse segments (Fig. 12a, b). The transfer of deformation from one structure to the next one can be done in two ways:

- The gradual decrease in thrusting offset is taken up by a gradual increase of dextral offset along the adjacent strike-slip fault (situation 1, Fig. 12a, b). This situation is best exemplified by the Split-Karlovac fault system, where branches b2-b4 and the fault at the western margin of the Tomislavgrad basin transfer their deformation in such a way that individual faults have low (hundreds of metres to few kilometres) offset to the NNW, while increasing to 10–15 km in the transfer zones and further SSE-wards (Fig. 5a);

- The gradual decrease in reverse offset is taken up by a gradual increase in offset along an opposite vergent reverse segments connected

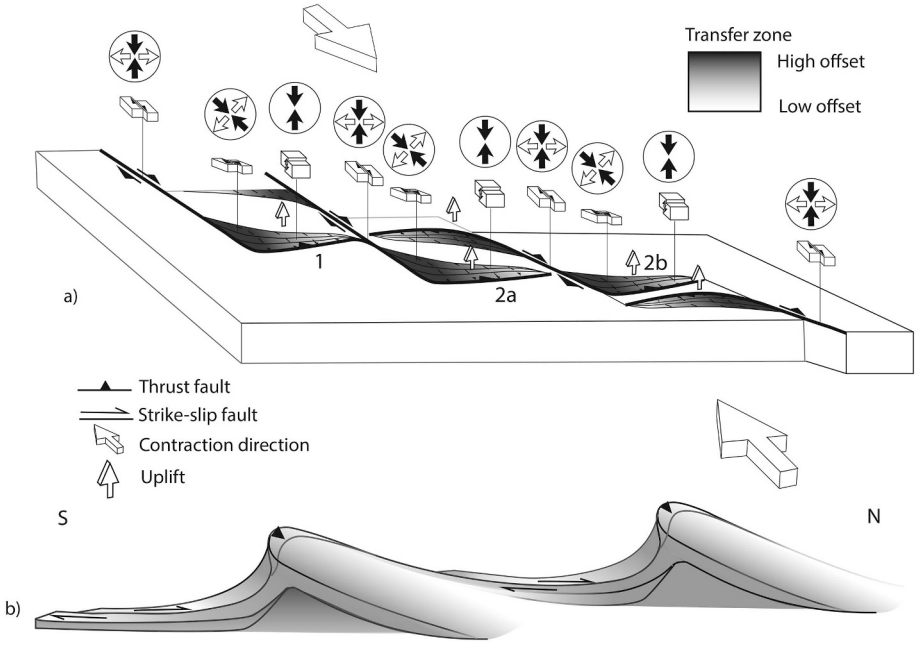

Fig. 12. Cartoons illustrating structural mechanisms of strain partitioning and transfer depicted by our study for the post- 9 Ma deformation event. a) 3D view of strain transfer between dextral strike-slip faults via restraining step-overs and/or restraining bends. The transfer of deformation between strike-slip faults is achieved in two ways: 1) a gradual decrease in thrusting offset is taken up by a gradual increase of dextral offset along the adjacent strike-slip fault; 2) a gradual decrease in reverse offset is taken up by a gradual increase in offset along an opposite vergent reverse fault connected with one other dextral strike-slip fault; b) 3D view of offset transfer between two reverse faults via a dextral strike-slip fault.

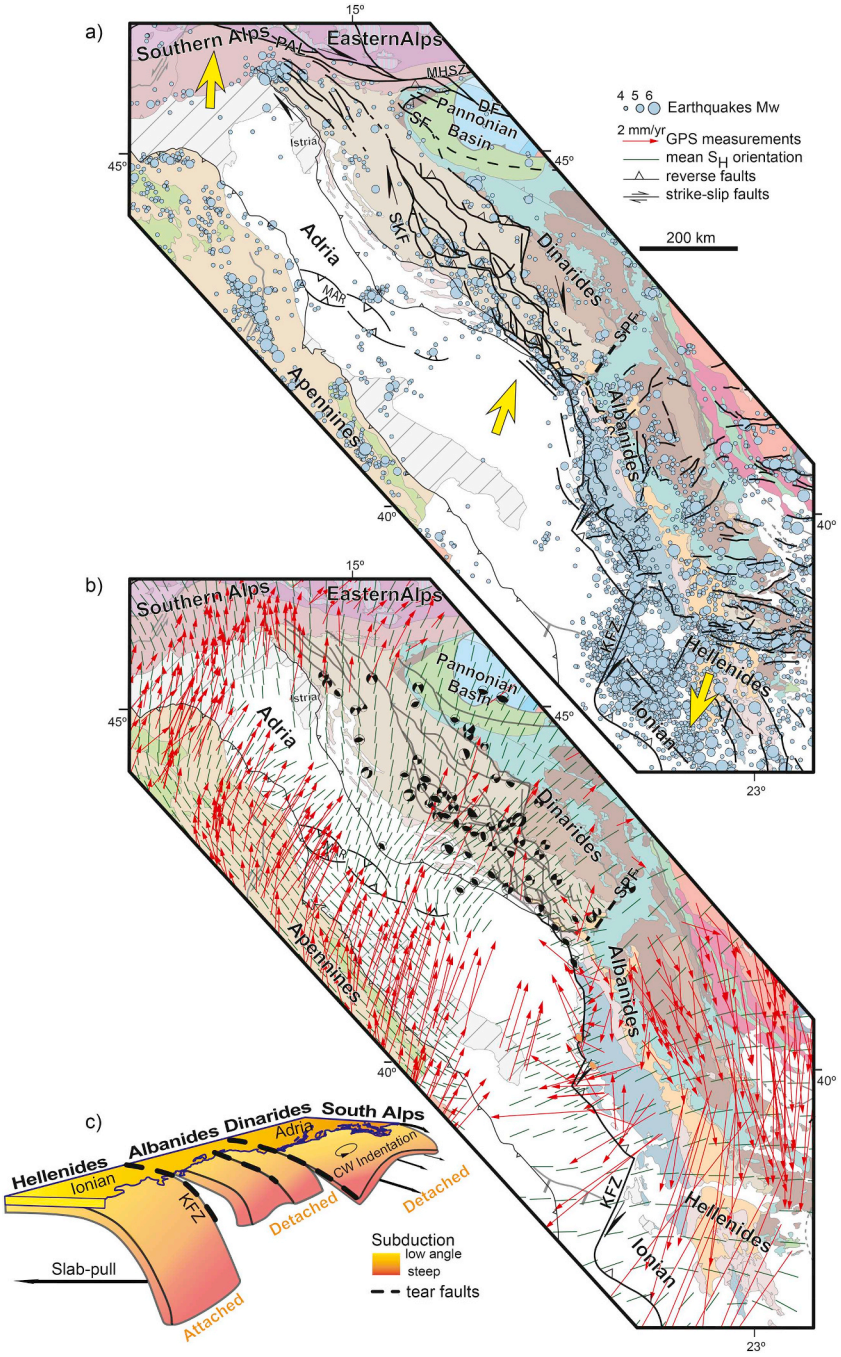

Fig. 13. The post- 9 Ma deformation mapped in the studied Dinarides area correlated in the larger Alps-Dinarides-Albanides-Hellenides-Apennines context. a) Tectonic map of the Dinarides and neighbouring orogens (adapted from Schmid et al., 2008; Schmid et al., 2011, legend and conventions presented in Fig. 1) overlaid by the post- 9 Ma deformation, and seismicity. The post- 9 Ma fault pattern in the Dinarides, Pannonian Basin, Southern and Eastern Alps is taken from our results and previous studies (Heberer et al., 2017; Moulin et al., 2016; Tomljenović and Csontos, 2001; Tomljenovic et al., 2008; Ustaszewski et al., 2014; van Gelder et al., 2015; Vrabec and Fodor, 2006; Vrabec et al., 2006). Presently active seismogenic faults are displayed in the Albanides and Hellenides (Caputo et al., 2012; Pavlides et al., 2010; Pérouse et al., 2017). Only the orogenic front is displayed in the Apennines. Only earthquakes with magnitude greater than 4 are displayed, their location is taken from the USGS earthquakes catalogue (https://earthquake.usgs.gov/earthquakes/), corrected by local studies whenever available (e.g., Herak et al., 2009; Pérouse et al., 2017). SKF = Split – Karlovac Fault; KFZ = Kefalonia Fault Zone; SPF = Skutari – Pec Fault; PAL = Peri-Adriatic Lineament; SF = Sava Fault; DF = Drava Fault; MHSZ = Mid-Hungarian Shear Zone; MAR = Middle Adriatic Ridge; b) The same tectonic map as in Fig. 13a (same conventions) overlaid by the present-day stress distribution and GPS horizontal motions. The GPS horizontal motions are displayed in an Eurasian fixed reference framework (D'Agostino et al., 2008; Grenerczy et al., 2005; Jouanne et al., 2012; Métois et al., 2015; Nocquet, 2012). The mean present-day maximum horizontal stress orientation (S_H) is compiled from previous studies (Bada et al., 2007; Heidbach et al., 2007; Heidbach et al., 2010; Pierdominici and Heidbach, 2012). The focal mechanisms are plotted only for calculated earthquakes in the Dinarides (after Sani et al., 2016 and references therein); c) Conceptual cartoon illustrating the lateral transition in the subduction and collision system between the Dinarides, Albanides and Hellenides. The cartoon infers subduction of continental mantle lithosphere disconnected from an oceanic slab by the Oligocene slab detachment beneath the Dinarides (Andrić et al., 2018), subduction of thinned continental lithosphere disconnected from an oceanic slab by previous slab detachment beneath the Albanides and subduction of oceanic and continental mantle lithosphere in a continuous Aegean slab beneath the Hellenides. The three areas are separated by slab tears. The cartoon also infers that the post- 9 Ma deformation accommodates the differential movement between the N- to NE-ward Adriatic indentation and continental subduction and the SW-ward movement driven by the Aegean slab pull.

with other dextral strike-slip segments along another curved faults (situations 2a and 2b, Fig. 12a). This situation is best exemplified along the Neretva Valley structure (NR in Fig. 7a). Here, dextral strike-slip faults connect to both a thick-skinned thrust and a thin-skinned backthrust (t1 and b1 in Fig. 3a, NR in Fig. 7a). These structures rapidly transfer their offsets between each other in such a way that the thrust offset increases and is larger W-wards, while the backthrust offset increases and is larger E-wards (which is the situation of the cross-section in Fig. 3a). This also indicates that deformation is transferred between thin-skinned and thick-skinned faults along dextral faults that function as lateral or oblique ramps.

The overall transfer of deformation allows for a gradual shift of shortening from more internal areas to the NE to more external to the SW by moving gradually the location of large-offset reverse faults towards the southern foreland (Fig. 12b). The WNW-ESE to N-S oriented large offsets dextral strike-slip faults may be interpreted as lateral or oblique ramps accommodating the transfer of shortening across an inherited NW-SE oriented nappe stack. High amounts of cumulative offset recorded by the system of curved dextral to reverse faults are observed in the Bosnian Flysch and the Budva unit of Montenegro. These areas contain deep-water to pelagic sediments, which are rheologically weaker when compared with the Paleozoic basement and Mesozoic shallow-water carbonatic cover deposited in the neighbouring units. As these areas have always recorded much larger amounts of deformation when compared with elsewhere in the external part of the Dinarides, this strain localisation is likely the result of focussing deformation in rheologically weak zones (see also van Unen et al., 2019).

The overall transfer mechanisms from strike-slip to high-angle reverse faulting can be described as a special class of continental restraining bends or stepovers (e.g., Biddle and Christie-Blick, 1985;

Cunningham and Mann, 2007 and references therein). As long as the rheology of rocks affected by deformation is homogenous, such as the typical High-Karst shallow water carbonate platform overlying the Variscan basement and Permian – lowermost Triassic clastics, the strike-slip deformation is dominant and transfers its offset between various fault branches across shorter segments of high-angle reverse faults. Whenever inherited weakness zones with a favourable orientation are present, such as the Bosnian Flysch or the Budva unit, deformation localizes in thrusts or oblique reverse faults that are dominant over shorter segments of strike-slip faulting.

In this kinematic (i.e. strain-based) framework, a first order interpretation of the three average paleostress solutions, obtained earlier by inverting faults belonging to the same deformation set can be provided in the larger context of the Dinarides (Fig. 12a). Taking the N- to N*E*-ward movement of the Adriatic microplate as a fixed (i.e. independent) strain constraint, the calculated average stresses can be seen as a dependent material response to this imposed boundary condition (e.g., Tikoff and Wojtal, 1999). In this framework, the N-S to NNE-SSW compressional stress reflects stress calculations by inverting measurements of reverse kinematics along E-W oriented, large-offset faults. The strike-slip stress field with N-S to NNE-SSW oriented compression reflects stress calculations by inverting measurements of dextral offsets (and their conjugate sinistral ones) in areas where the large offset faults change their strike to NW-SE to NNW-SSE. We interpret the strike-slip stress field with NW-SE oriented compression as a local effect that shows stress calculations by measurements of deformation in local areas connecting the earlier described dextral and reverse offsets along the same fault (Fig. 12a). The distribution of the measured kinematics corresponds, at regional scale, with this stress partitioning.

7. Towards understanding the post- 9 Ma Dinarides deformation in a larger geodynamic context

The patterns of post- 9 Ma deformation mapped across the central and south-eastern Dinarides partly fit the overall framework of Adriatic indentation, as defined by many previous studies (Fig. 13a,b, e.g., Handy et al., 2010; Pinter et al., 2005). The curved faults system with E-W to ESE-WNW oriented reverse segments and WNW-ESE to N-S oriented dextral segments is in general agreement with the overall N- to NE- ward direction of Adriatic movement derived by GPS studies in the Dinarides in respect to a stable European framework (Fig. 13b, e.g., D'Agostino et al., 2008; Grenerczy et al., 2005; Métois et al., 2015). While GPS movement vectors are oriented more N-wards in the NW Dinarides and the neighbouring Southern Alps, this movement gradually changes to NNE and NE towards the Pannonian Basin and the central and south-eastern part of the Dinarides (Fig. 13b). Across the Adriatic Sea, GPS studies indicate a N- to NE-ward movement of the Apennines along trajectories that can be generally connected with the ones observed in the Dinarides, Pannonian Basin, and Southern and Eastern Alps (Fig. 13b). The situation changes in the SE located Ionian domain, starting with the Albanides that record a ~1–5 mm/yr motion towards the NW in their external and towards the SE in their internal parts, while the Hellenides record much larger motions of ~10–36 mm/year, gradually rotating from S- to SW-ward following the structural vergence of the orogen in the overall direction of the Aegean slab-roll back (Jouanne et al., 2012; Kahle et al., 2000; Métois et al., 2015; Nocquet, 2012).

The N-S to NNE-SSW direction of compression derived by our regional average paleostress solutions is also in general agreement with modelled averages of the present-day maximum horizontal stress (S_H) field in the Dinarides (Fig. 13b). This modelled stress component indicates a gradual change from N-S orientations in the NW to NE-SW orientations in the SE Dinarides, which is compatible with the overall Adria indentation (Bada et al., 2007; Heidbach et al., 2007; Heidbach et al., 2010). Towards the Hellenides, this stress field changes to more E-W directions, which is a combined effect of a similarly oriented compression in external areas and perpendicular N-S to NNE-SSW oriented extensional deformation elsewhere, inferred to be the result of the S- to SSW-wards slab roll-back combined with gravitational spreading of the Aegean lithosphere (Heidbach et al., 2007; Konstantinou et al., 2017). A similar situation is observed in the Apennines (Fig. 13b), where the NW-SE S_H orientations are the result of a NE-SW oriented extension. To the NW of the Apennines, the S_H orientation gradually changes to NE-SW in the Adriatic Sea, interpreted to be a combination between horizontal gradients of the gravitational potential energy, the long-wavelength of the Africa-Europe convergence zone and the Adriatic indentation (Métois et al., 2015; Pierdominici and Heidbach, 2012).

Larger clusters of earthquakes are observed in the central Dinarides and the SE Budva zone in areas that are spatially juxtaposed over the mapped post- 9 Ma fault system (Fig. 13a). Focal mechanisms (plotted in Fig. 13b only for calculated Dinarides solutions) indicate either strike-slip or compressional solutions with N-S to NE-SW oriented P axes, which is in very good agreement with our observed kinematics and regional average paleostress solutions. Therefore, it is very likely that many faults that belong to our observed post- 9 Ma system are seismically active, although more precise localisation of this seismicity in local studies is generally scarce (Fig. 13a, see also Bada et al., 2007; Herak et al., 2009; Šumanovac et al., 2017; Ustaszewski et al., 2014).

In this overall context, it is rather clear that the post- 9 Ma fault system mapped in the central and SE part of the Dinarides accommodates the differential motion between the N- to NE-ward motion of Adria and the S- to SW-ward movement of the Hellenides and SE Albanides, driven by the roll-back of the Aegean slab. How exactly the deformation connects between the Alps and the Albanides-Hellenides? This is a difficult question given the local nature and problematic age of faults in many kinematic studies across the entire system. To the NW (Fig. 13a), a significant number of NW-SE to WNW-ESE oriented larger offsets dextral strike-slip faults, associated with E-W to ENE-WSW oriented reverse faults and smaller offset NE-SW to NNE-SSW oriented sinistral strike-slip faults has been mapped to be either latest Miocene – Quaternary, Pliocene-Quaternary or as a result of active and neotectonic deformation along the Peri-Adriatic Lineament or southwards in the NW-most part of the Dinarides (e.g., Heberer et al., 2017; Moulin et al., 2016; Tomljenović and Csontos, 2001; Tomljenovic et al., 2008; Ustaszewski et al., 2014; van Gelder et al., 2015; Vrabec and Fodor, 2006; Vrabec et al., 2006). The northern part of this fault system connects with the latest Miocene – Quaternary deformation of the Mid-Hungarian Shear Zone, Sava and Drava faults (e.g., Fodor et al., 2005; Fodor et al., 1998), which are located N to NE of the faults mapped in our study (Fig. 13a). The southern part of the fault system (immediately north of the Istria peninsula, Fig. 13a) likely connects with or transfer deformation to our observed Split-Karlovac and Bosnian Flysch faults systems. The larger offset strike-slip and thrusting focussed in the external part of the High-Karst, Budva and Dalmatian units of the SE Dinarides connect with the late Miocene – Quaternary faults in the external parts of the onshore and offshore Albania (Ionian and pre-Apulian zones, possibly also Krasta-Cukali unit in Fig. 1, Bega, 2015; Roure et al., 2004; Vilasi et al., 2009). More to the SE towards the Hellenides (Fig. 13a), the active thrusting is focussed in the external-most part of the orogenic wedge, close to the main deformation front (Caputo et al., 2012; Pavlides et al., 2010; Pérouse et al., 2017). This thrusting is displaced by NNE-SSW oriented dextral faults, among which the largest is the seismically active Kefalonia Fault Zone, a fault that started its activity at ~5 Ma (Louvari et al., 1999; Menant et al., 2016; Pérouse et al., 2017).

The zones where the overall structural kinematics, GPS motions, present-day horizontal stress and seismicity distributions change across the entire Dinarides – Albanides – Hellenides orogens are the Kefalonia Fault zone and the Skutari – Pec (or Shkoder – Peja) Fault zone (Fig. 13a). The first fault zone is thought to be the surface expression of a young tear fault in the Aegean subduction system separating

subduction of continental crust to the NW from subduction of oceanic crust to the SE (Fig. 13b, Evangelidis, 2017; Pearce et al., 2012). The second fault zone is interpreted to be the expression of an older transformant fault that separated the Mesozoic carbonate facies evolution (e.g., Aubouin and Dercourt, 1975; Robertson and Shallo, 2000; Velaj et al., 1999) and shows significant Miocene normal faulting offset accommodating an increase in roll-back subduction to the SE (Le Breton et al., 2017; Schmitz et al., 2017; Handy et al., 2019) of a transitional Adriatic-Ionian continental lithosphere affected by significant normal faulting (Bega, 2015). Therefore, the post- 9 Ma large scale transpression and high-angle reverse faulting observed in the study area justifies a mechanism of Adriatic indentation characterized by a gradual transition between continental subduction and N- to NE-ward movement of the Dinarides, to subduction of oceanic subduction and slab roll-back in the Hellenides SE of the Kefalonia Fault (Fig. 13c, see also Handy et al., 2019). Subduction of thinned continental lithosphere is still taking place likely in the transitional area of the Albanides – Hellenides NW of the Kefalonia Fault, which connects the present orogenic growth of the Alps and Dinarides from the orogenic collapse of the Hellenides.

8. Conclusions

Among the many examples available worldwide, the Neogene evolution of the Adriatic microplate in the Mediterranean domain provides one of the best places to understand indentation effects in terms of the relationship between deep lithosphere and mantle processes and the structural evolution of neighbouring orogens. Understanding the interplay between various mechanisms invoked for the Adriatic indentation was hampered by the lack of structural and kinematic data in the Dinarides, an orogen situated at the critical transition between the Alps, Albanides and Hellenides, and across the Adriatic margin of the Apennines. Starting from the scarcely available information for the post-Paleogene evolution, we have re-visited the less known area of the central and south-eastern Dinarides by focussing on collecting a new kinematic dataset for structures formed during the Adriatic indentation that postdate the main orogenic evolution.

In agreement with previous studies, our data shows that the lower-middle Miocene sediments of the Dinarides Lake System have been deposited during a period of extension that affected the entire orogen across its strike. Furthermore, we demonstrate for the first time that extension was followed by a period where strike-slip deformation was intimately associated with reverse faulting and thrusting. Starting from the early-middle Miocene basins, we have mapped how WNW-ESE to N-S oriented dextral strike-slip faults transfer gradually their offsets to E-W to NNW-SSE oriented dextral transpressive faults and ultimately to E-W to WNW-ESE oriented thrusts and high-angle reverse faults.

The overall transfer mechanism from strike-slip to high-angle reverse faulting can be described as a special class of continental restraining bends or stepovers. As long as the rheology of rocks affected by deformation is homogenous, the strike-slip deformation is dominant and transfers its offset between various fault branches across shorter segments of high-angle reverse faults. Whenever large-scale inherited weakness zones with a favourable orientation are present, such as units containing deep-water sediments that recorded significant deformation during the previous orogenic evolution, deformation localizes in thrusts or oblique reverse faults that are dominant over shorter segments of strike-slip faults. Strike-slip faults transfer their offset to thrusts in such a way that the offset changes along their strikes.

The observation of the regional early-middle Miocene extension in the Dinarides infers that there were no indentation effects prior to 9 Ma in this orogen. The geodynamic mechanism driving this period of extension that gradually reduces its effects towards the external parts of the orogen and has maximum amplitudes during the ~17–15 Ma Miocene Climatic Optimum (Mandic et al., 2012; Sant et al., 2018) are still unclear. One can think of horizontal gradients of the gravitational potential energy, prolongation of the Pannonian back-arc extension far into the Dinarides, roll-back of a Dinarides slab, processes associated with the subduction zone, eduction post-dating the Oligocene slab-break off (e.g., Andrić et al., 2018; Matenco and Radivojević, 2012 and references therein), but all such hypotheses remain speculative given the available data.

The onset of indentation that started in the Dinarides at ~9 Ma was likely associated with a differential motion of Adria in respect to the S- to SW- ward movement of a Hellenides area situated SE of the Kefalonia Fault, driven by the Aegean slab-roll back, facilitated by the thinned continental to oceanic nature of the Ionian lithosphere involved in the subduction system. The system of strike-slip, reverse and thrust faults mapped in the Dinarides that likely continues or transfers its offset to the NW until the Southern Alps and to the SE in the external part of the Albanides is nothing else but a large-scale crustal horizontal drag zone accommodating ~150–200 km of differential motion between the Adriatic indentation and Aegean slab roll-back in post- 9 Ma times. Partitioning the deformation related to the Adriatic indentation in the Apennines and Hellenides may be certainly influenced by asthenospheric flow around subducted slabs and moments of slab tearing or detachment, as previously inferred (e.g., Faccenna et al., 2014; Király et al., 2018; Le Breton et al., 2017). But such studies are still qualitative because they ignore a correct quantification of the timing and complex geometry of deformation in the Dinarides and need to be re-visited.

Acknowledgements

This study was financed by IFP Energies Nouvelles, Rueil Malmaison, France and University of Utrecht, The Netherlands. The excellent suggestions of two anonymous reviewers have significantly improved the original manuscript by particularly focussing the methodology towards an improved interpretation. Bruno Tomljenović, Matija Vukovski (University of Zagreb, Croatia), Hazim Hrvatović (Federal Institute for Geology, Sarajevo, Bosnia and Herzegovina), Marinko Toljić and Milos Radonjić (University of Belgrade, Serbia) are acknowledged for their collaboration during fieldwork and understanding the evolution of the Dinarides. Mark Handy, Stefan Schmid and Kamil Ustaszewski are acknowledged for discussion and understanding the large-scale orogenic correlations. All kinematic data supporting the results in this paper are available in the Supplementary Appendix or can be obtained by contacting the corresponding author.

Appendix A. Supplementary data

Supplementary data to this article can be found online at https://doi.org/10.1016/j.gloplacha.2019.103027.

References

Andrić, N., Sant, K., Matenco, L., Mandic, O., Tomljenović, B., Pavelić, D., Hrvatović, H., Demir, V., Ooms, J., 2017. The link between tectonics and sedimentation in asymmetric extensional basins: inferences from the study of the Sarajevo-Zenica Basin. Mar. Pet. Geol. 83, 305–332.

Andrić, N., Vogt, K., Matenco, L., Cvetković, V., Cloetingh, S., Gerya, T., 2018. Variability of orogenic magmatism during Mediterranean-style continental collisions: a numerical modelling approach. Gondwana Res. 56, 119–134.

Angelier, J., 1979. Determination of the mean principal directions of stresses for a given fault population. Tectonophysics 116, 17–26.

Angelier, J., 1984. Tectonic analysis of fault slip data sets. J. Geophys. Res. 89, 5835–5848.

Aubouin, J., Dercourt, J., 1975. Les transversales dinariques dérivent-elles de paléofailles transformantes? C. R. Acad. Sci. 281, 347–350.

Aubouin, J., Blanchet, R., Cadet, J.-P., Celet, P., Charvet, J., Chorowicz, J., Cousin, M., Rampnoux, J.-P., 1970. Essai sur la géologie des Dinarides. Bull. Soc. Geol. Fr. 12, 1060–1095.

Bada, G., Horváth, F., Dövényi, P., Szafián, P., Windhoffer, G., Cloetingh, S., 2007. Present-day stress field and tectonic inversion in the Pannonian basin. Glob. Planet. Chang. 58, 165–180.

Balázs, A., Matenco, L., Magyar, I., Horváth, F., Cloetingh, S., 2016. The link between tectonics and sedimentation in back-arc basins: new genetic constraints from the analysis of the Pannonian Basin. Tectonics 35, 1526–1559.

Bega, Z., 2015. Hydrocarbon exploration potential of Montenegro – a brief review. J. Pet.

Geol. 38, 317–330.
Bennett, R.A., Hreinsdóttir, S., Buble, G., Bašic, T., Bacic, Ž., Marjanović, M., Casale, G., Gendaszek, A., Cowan, D., 2008. Eocene to present subduction of southern Adria mantle lithosphere beneath the Dinarides. Geology 36, 3–6.
Bertotti, G., Mosca, P., Juez, J., Polino, R., Dunai, T., 2006. Oligocene to present kilometres scale subsidence and exhumation of the Ligurian Alps and the Tertiary Piedmont Basin (NW Italy) revealed by apatite (U-Th)/He thermochronology: correlation with regional tectonics. Terra Nova 18, 18–25.
Biddle, K.T., Christie-Blick, N., 1985. Strike-slip deformation, basin formation, and sedimentation. SEPM Soc. Sediment. Geol. 37, 1–34.
Burov, E., Francois, T., Agard, P., Le Pourhiet, L., Meyer, B., Tirel, C., Lebedev, S., Yamato, P., Brun, J.-P., 2014. Rheological and geodynamic controls on the mechanisms of subduction and HP/UHP exhumation of crustal rocks during continental collision: insights from numerical models. Tectonophysics 631, 212–250.
Cadjenovic, D., Kilibarda, Z., Radulovic, N., 2008. Late Triassic to Late Jurassic evolution of the Adriatic carbonate platform and Budva Basin, southern Montenegro. Sediment Geol. 204, 1–17.
Caporali, A., Aichhorn, C., Barlik, M., Becker, M., Fejes, I., Gerhatova, L., Ghitau, D., Grenerczy, G., Hefty, J., Krauss, S., Medak, D., Milev, G., Mojzes, M., Mulic, M., Nardo, A., Pesec, P., Rus, T., Simek, J., Sledzinski, J., Solaric, M., Stangl, G., Stopar, B., Vespe, F., Virag, G., 2009. Surface kinematics in the Alpine-Carpathian-Dinaric and Balkan region inferred from a new multi-network GPS combination solution. Tectonophysics 474, 295–321.
Caputo, R., Chatzipetros, A., Pavlides, S., Sboras, S., 2012. The greek database of seismogenic sources (GreDaSS): state-of-the-art for northern Greece. Ann. Geophys. 55, 859–894.
Célérier, B., Etchecopar, A., Bergerat, F., Vergely, P., Arthaud, F., Laurent, P., 2012. Inferring stress from faulting: from early concepts to inverse methods. Tectonophysics 581, 206–219. https://doi.org/10.1016/j.tecto.2012.02.009.
Chorowicz, J., 2016. Genesis of the Pieniny Klippen Belt in the Carpathians: possible effects of a major paleotransform fault in the Neo-Tethyan domain. Compt. Rendus Geosci. 348, 15–22.
Crne, A.E., Weissert, H., Gorican, S., Bernasconi, S.M., 2011. A biocalcification crisis at the Triassic-Jurassic boundary recorded in the Budva Basin (Dinarides, Montenegro). Geol. Soc. Am. Bull. 123, 40–50.
Cunningham, W.D., Mann, P., 2007. Tectonics of strike-slip restraining and releasing bends. Geol. Soc. Lond. Spec. Publ. 290, 1.
D'Agostino, N., Avallone, A., Cheloni, D., D'Anastasio, E., Mantenuto, S., Selvaggi, G., 2008. Active tectonics of the Adriatic region from GPS and earthquake slip vectors. J. Geophys. Res. Solid Earth 113. https://doi.org/10.1029/2008JB005860.
Dahlstrom, C.D.A., 1969. Balanced cross sections. Canadian Journal of Earth Sciences 6 (4), 743–757. https://doi.org/10.1139/e69-069.
Davy, P., Cobbold, P.R., 1988. Indentation tectonics in nature and experiment. 1. Experiments scaled from gravity. Bull. Geol. Inst. Uppsala 14, 129–141.
de Leeuw, A., Mandic, O., Vranjkovic, A., Pavelic, D., Harzhauser, M., Krijgsman, W., Kuiper, K.F., 2010. Chronology and integrated stratigraphy of the Miocene Sinj Basin (Dinaride Lake System, Croatia). Paleogeogr. Paleoclimatol. Paleoecol. 292, 155–167.
de Leeuw, A., Mandic, O., Krijgsman, W., Kuiper, K.F., Hrvatović, H., 2011. A chronostratigraphy for the Dinaride Lake System deposits of the Livno-Tomislavgrad Basin: the rise and fall of a long-lived lacustrine environment. Stratigraphy 8, 29–43.
de Leeuw, A., Mandic, O., Krijgsman, W., Kuiper, K., Hrvatović, H., 2012. Paleomagnetic and geochronologic constraints on the geodynamic evolution of the Central Dinarides. Tectonophysics 530-531, 286–298.
De Vicente, G., Vegas, R., Muñoz-Martín, A., Van Wees, J.D., Casas-Sáinz, A., Sopeña, A., Sánchez-Moya, Y., Arche, A., López-Gómez, J., Olaiz, A., Fernández-Lozano, J., 2009. Oblique strain partitioning and transpression on an inverted rift: the Castilian Branch of the Iberian Chain. Tectonophysics 470, 224–242.
Delvaux, D., Sperner, B., 2003. Stress tensor inversion from fault kinematic indicators and focal mechanism data: the TENSOR program. In: Nieuwland, D. (Ed.), New Insights into Structural Interpretation and Modelling. 212. Geological Society, London, Special Publications, pp. 75–100.
Dimitrijević, M.D., 1997. Geology of Yugoslavia, 2nd ed. Geoinstitute, Belgrade 187 pp.
Dimitrijevic, M.D., 2001. Dinarides and the Vardar Zone: a short review of the geology. Acta Vulcanol. 13, 1–8.
Doglioni, C., Carminati, E., Cuffaro, M., Scrocca, D., 2007. Subduction kinematics and dynamic constraints. Earth-Sci. Rev. 83, 125–175.
Duretz, T., Gerya, T.V., 2013. Slab detachment during continental collision: influence of crustal rheology and interaction with lithospheric delamination. Tectonophysics 602, 124–140.
Erak, D., Matenco, L., Toljić, M., Stojadinović, U., Andriessen, P.A.M., Willingshofer, E., Ducea, M.N., 2017. From nappe stacking to extensional detachments at the contact between the Carpathians and Dinarides – the Jastrebac Mountains of Central Serbia. Tectonophysics 710–711, 162–183.
Evangelidis, C.P., 2017. Seismic anisotropy in the Hellenic subduction zone: effects of slab segmentation and subslab mantle flow. Earth Planet. Sci. Lett. 480, 97–106.
Faccenna, C., Becker, T.W., 2010. Shaping mobile belts by small-scale convection. Nature 465, 602–605.
Faccenna, C., Piromallo, C., Crespo-Blanc, A., Jolivet, L., Rosetti, F., 2004. Lateral slab deformation and the origin of the western Mediterranean arcs. Tectonics 23, TC1012. https://doi.org/10.1029/2002TC001488.
Faccenna, C., Becker, T.W., Auer, L., Billi, A., Boschi, L., Brun, J.P., Capitanio, F.A., Funiciello, F., Horvàth, F., Jolivet, L., Piromallo, C., Royden, L., Rossetti, F., Serpelloni, E., 2014. Mantle dynamics in the Mediterranean. Rev. Geophys. 52, 283–332.
Fodor, L., Jelen, B., Marton, E., Skaberne, D., Car, J., Vrabec, M., 1998. Miocene-Pliocene evolution of the Slovenian Periadriatic fault: implications for the Carpathians extrusion models. Tectonics 17, 690–709.
Fodor, L., Bada, G., Csillag, G., Horvath, E., Ruszkiczay-Rudiger, Z., Palotas, K., Sikhegyi, F., Timar, G., Cloetingh, S., 2005. An outline of neotectonic structures and morphotectonics of the western and central Pannonian Basin. Tectonophysics 410, 15–41.
Frisch, W., Dunkl, I., Kuhlemann, J., 2000. Post-collisional orogen-parallel large-scale extension in the Eastern Alps. Tectonophysics 327, 239–265.
Gorican, S., 1994. Jurassic and Cretaceous radiolarian biostratigraphy and sediemntary evolution of the Budva Zone (Dinarides, Montenegro). Mem. Geol. 18 Lausanne, 177 pp.
Goričan, Š., Košir, A., Rožič, B., Šmuc, A., Gale, L., Kukoč, D., Celarc, B., Črne, A.E., Kolar-Jurkovšek, T., Placer, L., 2012. Mesozoic deep-water basins of the eastern Southern Alps (NW Slovenia). J. Alpine Geol. 55, 1–44.
Grenerczy, G., Sella, G., Stein, S., Kenyeres, A., 2005. Tectonic implications of the GPS velocity field in the northern Adriatic region. Geophys. Res. Lett. 32. https://doi.org/10.1029/2005GL022947.
Handy, M.R., Schmid, M., Bousquet, R., Kissling, E., Bernoulli, D., 2010. Reconciling plate-tectonic reconstructions of Alpine Tethys with the geological-geophysical record of spreading and subduction in the Alps. Earth-Sci. Rev. 102, 121–158.
Handy, M.R., Ustaszewski, K., Kissling, E., 2014. Reconstructing the Alps–Carpathians–Dinarides as a key to understanding switches in subduction polarity, slab gaps and surface motion. Int. J. Earth Sci. 104, 1–26.
Handy, M.R., Giese, J., Schmid, S.M., Pleuger, J., Spakman, W., Onuzi, K., Ustaszewski, K., 2019. Coupled crust-mantle response to slab tearing, bending, and rollback along the Dinaride-Hellenide orogen. Tectonics 38. https://doi.org/10.1029/2019TC005524.
Harzhauser, M., Mandic, O., 2008. Neogene lake systems of Central and South-Eastern Europe: faunal diversity, gradients and interrelations. Paleogeogr. Paleoclimatol. Paleoecol. 260, 417–434.
Harzhauser, M., Mandic, O., Latal, C., Kern, A., 2011. Stable isotope composition of the Miocene Dinaride Lake System deduced from its endemic mollusc fauna. Hydrobiologia 682, 27–46.
Heberer, B., Reverman, R.L., Fellin, M.G., Neubauer, F., Dunkl, I., Zattin, M., Seward, D., Genser, J., Brack, P., 2017. Postcollisional cooling history of the Eastern and Southern Alps and its linkage to Adria indentation. Int. J. Earth Sci. 106, 1557–1580.
Heidbach, O., Reinecker, J., Tingay, M., Müller, B., Sperner, B., Fuchs, K., Wenzel, F., 2007. Plate boundary forces are not enough: second- and third-order stress patterns highlighted in the World Stress Map database. Tectonics 26.
Heidbach, O., Tingay, M., Barth, A., Reinecker, J., Kurfess, D., Muller, B., 2010. Global crustal stress pattern based on the World Stress Map database release 2008. Tectonophysics 482, 3–15.
Heidbach, O., Rajabi, M., Cui, X., Fuchs, K., Müller, B., Reinecker, J., Reiter, K., Tingay, M., Wenzel, F., Xie, F., Ziegler, M.O., Zoback, M.-L., Zoback, M., 2018. The World Stress Map database release 2016: crustal stress pattern across scales. Tectonophysics 744, 484–498.
Herak, D., Herak, M., Tomljenovic, B., 2009. Seismicity and earthquake focal mechanisms in North-Western Croatia. Tectonophysics 465, 212–220.
Hippolyte, J.-C., Bergerat, F., Gordon, M.B., Bellier, O., Espurt, N., 2012. Key and pitfalls in mesoscale fault analysis and paleostress reconstructions, the use of Angelier's methods. Tectonophysics 581, 144–162. https://doi.org/10.1016/j.tecto.2012.01.012.
Horváth, F., Musitz, B., Balázs, A., Végh, A., Uhrin, A., Nádor, A., Koroknai, B., Pap, N., Tóth, T., Wórum, G., 2015. Evolution of the Pannonian basin and its geothermal resources. Geothermics 53, 328–352.
Houseman, G., England, P., 1993. Crustal thickening versus lateral expulsion in the Indian-Asian continental collision. J. Geophys. Res. Solid Earth 98, 12233–12249.
Hrvatović, H., 2006. Geological Guidebook through Bosnia and Herzegovina. Geological Survey of Federation Bosnia and Herzegovina, Sarajevo 172 pp.
Hrvatović, H., Pamić, J., 2005. Principal thrust-nappe structures of the Dinarides. Acta Geol. Hung. 48 (2), 133–151.
Jolivet, L., Brun, J.-P., 2010. Cenozoic geodynamic evolution of the Aegean. Int. J. Earth Sci. 99, 109–138.
Jolivet, L., Menant, A., Sternai, P., Rabillard, A., Arbaret, L., Augier, R., Laurent, V., Beaudoin, A., Grasemann, B., Huet, B., Labrousse, L., Le Pourhiet, L., 2015. The geological signature of a slab tear below the Aegean. Tectonophysics 659, 166–182.
Jolivet, L., Faccenna, C., Becker, T., Tesauro, M., Sternai, P., Bouilhol, P., 2018. Mantle flow and deforming continents: from India-Asia convergence to Pacific subduction. Tectonics 37, 2887–2914.
Jones, R.R., Tanner, G.P.W., 1995. Strain partitioning in transpression zones. J. Struct. Geol. 17, 793–802.
Jouanne, F., Mugnier, J.L., Koci, R., Bushati, S., Matev, K., Kuka, N., Shinko, I., Kociu, S., Duni, L., 2012. GPS constraints on current tectonics of Albania. Tectonophysics 554-557, 50–62.
Kahle, H.G., Cocard, M., Peter, Y., Geiger, A., Reilinger, R., Barka, A., Veis, G., 2000. GPS-derived strain rate field within the boundary zones of the Eurasian, African, and Arabian Plates. J. Geophys. Res. Solid Earth 105, 23353–23370.
Király, Á., Faccenna, C., Funiciello, F., 2018. Subduction zones interaction around the Adria microplate and the origin of the Apenninic Arc. Tectonics 37, 3941–3953.
Kissling, E., Schmid, S.M., Lippitsch, R., Ansorge, J., Fugenschuh, B., 2006. Lithosphere structure and tectonic evolution of the Alpine arc: new evidence from high-resolution teleseismic tomography. Geol. Soc. Lond. Mem. 32, 129–145.
Konstantinou, K.I., Mouslopoulou, V., Liang, W.T., Heidbach, O., Oncken, O., Suppe, J., 2017. Present-day crustal stress field in Greece inferred from regional-scale damped inversion of earthquake focal mechanisms. J. Geophys. Res. Solid Earth 122, 506–523.

Korbar, T., 2009. Orogenic evolution of the external Dinarides in the NE Adriatic region: a model constrained by tectonostratigraphy of Upper Cretaceous to Paleogene carbonates. Earth-Sci. Rev. 96, 296–312.
Lacombe, O., 2012. Do fault slip data inversions actually yield "paleostresses" that can be compared with contemporary stresses? A critical discussion. Compt. Rendus Geosci. 344, 159–173.
Lancaster, P., Salkauskas, K., 1981. Surfaces generated by moving least-squares methods. Math. Comput. 37, 141–158.
Le Breton, E., Handy, M.R., Molli, G., Ustaszewski, K., 2017. Post-20 Ma motion of the Adriatic Plate: new constraints from surrounding orogens and implications for crust-mantle decoupling. Tectonics 36, 3135–3154.
Lisle, R., 2013. A critical look at the Wallace-Bott hypothesis in fault-slip analysis. Bulletin de la Societe Geologique de France 184, 299–306. https://doi.org/10.2113/gssgfbull.184.4-5.299.
Louvari, E., Kiratzi, A.A., Papazachos, B.C., 1999. The Cephalonia Transform Fault and its extension to western Lefkada Island (Greece). Tectonophysics 308, 223–236.
Magyar, I., Geary, D.H., 2012. Biostratigraphy in a Late Neogene Caspian-type lacustrine basin: Lake Pannon, Hungary. In: Baganz, O.W., Bartov, Y., Bohacs, K., Nummedal, D. (Eds.), Lacustrine Sandstone Reservoirs and Hydrocarbon Systems. AAPG Memoir 95. pp. 255–264.
Mandic, O., de Leeuw, A., Vukovic, B., Krijgsman, W., Harzhauser, M., Kuiper, K.F., 2011. Palaeoenvironmental evolution of Lake Gacko (Southern Bosnia and Herzegovina): impact of the middle miocene climatic optimum on the Dinaride Lake System. Paleogeogr. Paleoclimatol. Paleoecol. 299, 475–492.
Mandic, O., de Leeuw, A., Bulić, J., Kuiper, K.F., Krijgsman, W., Jurišić-Polšak, Z., 2012. Paleogeographic evolution of the Southern Pannonian Basin: 40Ar/39Ar age constraints on the Miocene continental series of Northern Croatia. Int. J. Earth Sci. 101, 1033–1046.
Mandic, O., Hajek-Tadesse, V., Bakrač, K., Reichenbacher, B., Grizelj, A., Miknić, M., 2019a. Multiproxy reconstruction of the middle Miocene Požega palaeolake in the Southern Pannonian Basin (NE Croatia) prior to the Badenian transgression of the Central Paratethys Sea. Paleogeogr. Paleoclimatol. Paleoecol. 516, 203–219.
Mandic, O., Sant, K., Kallanxhi, M.-E., Ćorić, S., Theobalt, D., Grunert, P., de Leeuw, A., Krijgsman, W., 2019b. Integrated bio-magnetostratigraphy of the Badenian reference section Ugljevik in southern Pannonian Basin – implications for the Paratethys history (middle Miocene, Central Europe). Glob. Planet. Chang. 172, 374–395.
Matenco, L., Radivojević, D., 2012. On the formation and evolution of the Pannonian Basin: constraints derived from the structure of the junction area between the Carpathians and Dinarides. Tectonics 31, TC6007.
Matenco, L., Krézsek, C., Merten, S., Schmid, S., Cloetingh, S., Andriessen, P., 2010. Characteristics of collisional orogens with low topographic build-up: an example from the Carpathians. Terra Nova 22, 155–165.
Matenco, L., Munteanu, I., ter Borgh, M., Stanica, A., Tilita, M., Lericolais, G., Dinu, C., Oaie, G., 2016. The interplay between tectonics, sediment dynamics and gateways evolution in the Danube system from the Pannonian Basin to the western Black Sea. Sci. Total Environ. 543 (Part A), 807–827.
Matenco, L., Bertotti, G., Leever, K., Cloetingh, S., Schmid, S.M., Tărăpoancă, M., Dinu, C., 2007. Large-scale deformation in a locked collisional boundary: Interplay between subsidence and uplift, intraplate stress, and inherited lithospheric structure in the late stage of the SE Carpathians evolution. TC4011. Tectonics 26. https://doi.org/10.1029/2006TC001951.
Meissner, R., Mooney, W., 1998. Weakness of the lower continental crust: a condition for delamination, uplift, and escape. Tectonophysics 296, 47–60.
Menant, A., Jolivet, L., Vrielynck, B., 2016. Kinematic reconstructions and magmatic evolution illuminating crustal and mantle dynamics of the eastern Mediterranean region since the late Cretaceous. Tectonophysics 675, 103–140.
Métois, M., D'Agostino, N., Avallone, A., Chamot-Rooke, N., Rabaute, A., Duni, L., Kuka, N., Koci, R., Georgiev, I., 2015. Insights on continental collisional processes from GPS data: dynamics of the peri-Adriatic belts. J. Geophys. Res. Solid Earth 120, 8701–8719.
Mikes, T., Christ, D., Petri, R., Dunkl, I., Frei, D., Báldi-Beke, M., Reitner, J., Wemmer, K., Hrvatović, H., von Eynatten, H., 2008. Provenance of the Bosnian Flysch. Swiss J. Geosci. 101, 31–54.
Milojevic, R., Sunaric, O., 1962. Geoloski prikaz lezista lignita Prolog u Livanjskom ugljenonosnom basenu (Geological investigation of lignite Prolog in the Livno coal basin). Geoloski glasnik 6, 85–101.
Milojević, R., Sunarić, O., 1964. Pokušaj stratigrafskog raščlanjavanja slatkovodnih sedimenata Duvanjskog basena i neki ekonomsko geološki momenti u razvoju ugljenih facija (An attempt to stratigraphically separate the freshwater sediments of the Duvanj basin and some economic and geological moments in the development of coal basin). Geološki glasnik 9, 59–75.
Molnar, P., Tapponnier, P., 1975. Cenozoic tectonics of Asia: effects of a continental collision. Science 189, 419–426.
Moulin, A., Benedetti, L., Rizza, M., Jamšek Rupnik, P., Gosar, A., Bourlès, D., Keddadouche, K., Aumaître, G., Arnold, M., Guillou, V., Ritz, J.-F., 2016. The Dinaric fault system: large-scale structure, rates of slip, and Plio-Pleistocene evolution of the transpressive northeastern boundary of the Adria microplate. Tectonics 35, 2258–2292.
Mrinjek, E., 1993. Sedimentology and depositional setting of alluvial Promina Beds in Northern Dalmatia. Geol. Croatica 46, 243–261.
Munteanu, I., Willingshofer, E., Matenco, L., Sokoutis, D., Cloetingh, S., 2014. Far-field contractional polarity changes in models and nature. Earth Planet. Sci. Lett. 395, 101–115.
Nocquet, J.-M., 2012. Present-day kinematics of the Mediterranean: a comprehensive overview of GPS results. Tectonophysics 579, 220–242.
Orife, T., Lisle, J., 2003. Numerical processing of paleostress results. J. Struct. Geol. 25, 949–957.
Pamic, J.J., 1984. Triassic magmatism of the Dinarides in Yugoslavia. Tectonophysics 109, 273–307.
Pamić, J., 2002. The Sava-vardar zone of the Dinarides and Hellenides versus the Vardar Ocean. Eclogae Geol. Helv. 95, 99–113.
Pantić, N.K., Bešlagić, A., 1964. Palinološke analize mrkog uglja i lignita iz Livanjskog tercijarnog bazena (Palinological analyzes of brown coal and lignite from the Livno Tertiary basin). Geol. An. Balk. Poluostrva 31, 127–133.
Pantić, N., Ercegovac, M., Pantić, V., 1966. Palinološka ispitivanja i stratigrafija terestrično-limničkih tercijarnih naslaga u Zeničko-Sarajevskom basenu (Palinological investigations and stratigraphy of terrestrial and limestone tertiary deposits in the Zenica-Sarajevo basin). Geol. An. Balk. Poluostrva 32, 183–210.
Pavelić, D., Kovačić, M., 2018. Sedimentology and stratigraphy of the Neogene rift-type North Croatian Basin (Pannonian Basin System, Croatia): a review. Mar. Pet. Geol. 91, 455–469.
Pavlides, S., Caputo, R., Sboras, S., Chatzipetros, A., Papathanasiou, G., Valkaniotis, S., 2010. The Greek catalogue of active faults and seismogenic sources. Bull. Geol. Soc. Greece 43, 486–494.
Pearce, F.D., Rondenay, S., Sachpazi, M., Charalampakis, M., Royden, L.H., 2012. Seismic investigation of the transition from continental to oceanic subduction along the western Hellenic Subduction Zone. J. Geophys. Res. Solid Earth 117.
Peral, M., Király, Á., Zlotnik, S., Funiciello, F., Fernàndez, M., Faccenna, C., Vergés, J., 2018. Opposite subduction polarity in adjacent plate segments. Tectonics 37, 3285–3302.
Pérouse, E., Sébrier, M., Braucher, R., Chamot-Rooke, N., Bourlès, D., Briole, P., Sorel, D., Dimitrov, D., Arsenikos, S., 2017. Transition from collision to subduction in Western Greece: the Katouna–Stamna active fault system and regional kinematics. Int. J. Earth Sci. 106, 967–989.
Picha, F., 2002. Late orogenic strike-slip faulting and escape tectonics in frontal Dinarides-Hellenides, Croatia, Yugoslavia, Albania, and Greece. AAPG Bull. 86, 1659–1671.
Picotti, V., Pazzaglia, F.J., 2008. A new active tectonic model for the construction of the Northern Apennines mountain front near Bologna (Italy). J. Geophys. Res. 113, B08412. https://doi.org/10.1029/2007jb005307.
Pierdominici, S., Heidbach, O., 2012. Stress field of Italy — mean stress orientation at different depths and wave-length of the stress pattern. Tectonophysics 532–535, 301–311.
Pinter, N., Grenerczy, G., Weber, J., Stein, S., Medak, D., 2005. The Adria Microplate: GPS Geodesy, Tectonics and Hazards (Nato Science Series: IV: Earth and Environmental Sciences). Springer 413 pp.
Ratschbacher, L., Frisch, W., Linzer, H.G., Merle, O., 1991. Lateral extrusion in the Eastern Alps; part 2, structural analysis. Tectonics 10, 257–271.
Regard, V., Faccenna, C., Martinod, J., Bellier, O., 2005. Slab pull and indentation tectonics: insights from 3D laboratory experiments. Phys. Earth Planet. Inter. 149, 99–113.
Robertson, A., Shallo, M., 2000. Mesozoic-Tertiary tectonic evolution of Albania in its regional Eastern Mediterranean context. Tectonophysics 316, 197–254.
Robertson, A., Karamata, S., Saric, K., 2009. Overview of ophiolites and related units in the Late Palaeozoic-Early Cenozoic magmatic and tectonic development of Tethys in the northern part of the Balkan region. Lithos 108, 1–36.
Rosenberg, C.L., Brun, J.P., Cagnard, F., Gapais, D., 2007. Oblique indentation in the Eastern Alps: insights from laboratory experiments. Tectonics 26.
Roure, F., GFili, I., Najaz, S., Cadet, J.P., Mushka, K., Bonneau, M., 2004. Kinematic evolution and petroleum systems—an appraisal of the outer Albanides. In: McClay, K.R. (Ed.), Thrust Tectonics and Hydrocarbon Systems. 82. AAPG Memoir, pp. 474–493.
Sani, F., Vannucci, G., Boccaletti, M., Bonini, M., Corti, G., Serpelloni, E., 2016. Insights into the fragmentation of the Adria Plate. J. Geodyn. 102, 121–138. https://doi.org/10.1016/j.jog.2016.09.004.
Sant, K., Andrić, N., Mandic, O., Demir, V., Pavelić, D., Rundić, L., Hrvatović, H., Matenco, L., Krijgsman, W., 2018. Magneto-biostratigraphy and paleoenvironments of the Miocene freshwater sediments of the Sarajevo-Zenica Basin. Paleogeogr. Paleoclimatol. Paleoecol. 506, 48–69.
Schefer, S., 2010. Tectono-Metamorphic and Magmatic Evolution of the Internal Dinarides (Kopaonik Area, Southern Serbia) and its Significance for the Geodynamic Evolution of the Balkan Peninsula. Universitat Basel, Basel 230 pp.
Schmid, S., Bernoulli, D., Fügenschuh, B., Matenco, L., Schefer, S., Schuster, R., Tischler, M., Ustaszewski, K., 2008. The Alpine-Carpathian-Dinaridic orogenic system: correlation and evolution of tectonic units. Swiss J. Geosci. 101, 139–183.
Schmid, S.M., Bernoulli, D., Fügenschuh, B., Matenco, L., Schefer, S., Oberhänsli, R., Ustaszewski, K., 2011. Tracing the closure of Neotethys from the Alps to Western Turkey II: similarities and differences between Dinarides, Hellenides and Anatolides-Taurides. Geophys. Res. Abstr. 13, EGU2011–4000.
Schmid, S.M., Kissling, E., Diehl, T., van Hinsbergen, D.J.J., Molli, G., 2017. Ivrea mantle wedge, arc of the Western Alps, and kinematic evolution of the Alps-Apennines orogenic system. Swiss J. Geosci. 110, 581–612.
Schmitz, B., Ustaszewski, K., Wemmer, K., Onuzi, K., Muceku, B., 2017. Kinematics and Age of the Orogen-Perpenticular Shkodër-Peja-Normal-Fault, Northern Albania, 13th Workshop on Alpine Geological Studies. Zlatibor, Serbia.
Scisciani, V., Calamita, F., 2009. Active intraplate deformation within Adria: examples from the Adriatic Region. Tectonophysics 476, 57–72. https://doi.org/10.1016/j.tecto.2008.10.030.
Simón, J.L., 2019. Forty years of paleostress analysis: has it attained maturity? J. Struct. Geo 125, 124–133. https://doi.org/10.1016/j.jsg.2018.02.011.
Smit, J.H.W., Cloetingh, S.A.P.L., Burov, E., Tesauro, M., Sokoutis, D., Kaban, M., 2013. Interference of lithospheric folding in western Central Asia by simultaneous Indian

and Arabian plate indentation. Tectonophysics 602, 176–193.
Sperner, B., Zweigel, P., 2010. A plea for more caution in fault-slip analysis. Tectonophysics 482, 29–41.
Stampfli, G.M., Borel, G.D., 2002. A plate tectonic model for the Paleozoic and Mesozoic constrained by dynamic plate boundaries and restored synthetic oceanic isochrons. Earth Planet. Sci. Lett. 196, 17–33.
Stojadinovic, U., Matenco, L., Andriessen, P., Toljić, M., Rundić, L., Ducea, M.N., 2017. Structure and provenance of Late Cretaceous–Miocene sediments located near the NE Dinarides margin: inferences from kinematics of orogenic building and subsequent extensional collapse. Tectonophysics 710–711, 184–204.
Šumanovac, F., 2010. Lithosphere structure at the contact of the Adriatic microplate and the Pannonian segment based on the gravity modelling. Tectonophysics 485 (1–4), 94–106. https://doi.org/10.1016/j.tecto.2009.12.005.
Šumanovac, F., Dudjak, D., 2016. Descending lithosphere slab beneath the Northwest Dinarides from teleseismic tomography. J. Geodyn. 102, 171–184.
Šumanovac, F., Markušić, S., Engelsfeld, T., Jurković, K., Orešković, J., 2017. Shallow and deep lithosphere slabs beneath the Dinarides from teleseismic tomography as the result of the Adriatic lithosphere downwelling. Tectonophysics 712, 523–541.
Šušnjara, A., Sakač, K., Jelen, B., Gabrić, A., 1992. Upper Permian evaporites and associated rocks of Dalmatia and Borderline Area of Lika and Bosnia. Geol. Croatica 45, 95–114.
Tari, V., 2002. Evolution of the northern and western Dinarides: a tectonostratigraphic approach. In: Bertotti, G., Cloetingh, S. (Eds.), Neotectonics and Surface Processes: The Pannonian Basin and Alpine/Carpathian System. EGU Special Publication, pp. 105–120.
Tari, V., Mrinjek, E., 1994. The role of palaeogene clastics in the tectonic interpretation of northern Dalmatia (southern Croatia). Geol. Croatica 1, 127–138.
Tikoff, B., Wojtal, S.F., 1999. Displacement control of geologic structures. J. Struct. Geol. 21, 959–967. https://doi.org/10.1016/S0191-8141(99)00045-0.
Tišljar, J., 1992. Origin and depositional environments of the evaporite and carbonate complex (Upper Permian) from the central part of the Dinarides (Southern Croatia and Western Bosnia). Geol. Croatica 45, 115–126.
Toljić, M., Matenco, L., Ducea, M.N., Stojadinović, U., Milivojević, J., Đerić, N., 2013. The evolution of a key segment in the Europe–Adria collision: the Fruška Gora of northern Serbia. Glob. Planet. Chang. 103, 39–62.
Toljić, M., Matenco, L., Stojadinović, U., Willingshofer, E., Ljubović-Obradović, D., 2018. Understanding fossil fore-arc basins: inferences from the Cretaceous Adria-Europe convergence in the NE Dinarides. Glob. Planet. Chang. 171, 167–184.
Tomljenović, B., Csontos, L., 2001. Neogene-Quaternary structures in the border zone between Alps, Dinarides and Pannonian Basin (Hrvatsko zagorje and Karlovac Basins, Croatia). Int. J. Earth Sci. V90, 560–578.
Tomljenovic, B., Csontos, L.s., Márton, E., Márton, P., 2008. Tectonic evolution of the northwestern Internal Dinarides as constrained by structures and rotation of Medvednica Mountains, North Croatia. Geol. Soc. Lond. Spec. Publ. 298, 145–167.
Ustaszewski, K., Schmid, S., Fügenschuh, B., Tischler, M., Kissling, E., Spakman, W., 2008. A map-view restoration of the Alpine-Carpathian-Dinaridic system for the Early Miocene. Swiss J. Geosci. 101, 273–294.
Ustaszewski, K., Schmid, S.M., Lugovic, B., Schuster, R., Schaltegger, U., Bernoulli, D., Hottinger, L., Kounov, A., Fügenschuh, B., Schefer, S., 2009. Late Cretaceous intra-oceanic magmatism in the internal Dinarides (northern Bosnia and Herzegovina): implications for the collision of the Adriatic and European plates. Lithos 108, 106–125.
Ustaszewski, K., Kounov, A., Schmid, S.M., Schaltegger, U., Krenn, E., Frank, W., Fügenschuh, B., 2010. Evolution of the Adria-Europe plate boundary in the northern Dinarides: from continent-continent collision to back-arc extension. Tectonics 29, TC6017. https://doi.org/10.1029/2010tc002668.
Ustaszewski, K., Herak, M., Tomljenović, B., Herak, D., Matej, S., 2014. Neotectonics of the Dinarides–Pannonian Basin transition and possible earthquake sources in the Banja Luka epicentral area. J. Geodyn. 82, 52–68.
van Gelder, I.E., Matenco, L., Willingshofer, E., Tomljenović, B., Andriessen, P.A.M., Ducea, M.N., Beniest, A., Gruić, A., 2015. The tectonic evolution of a critical segment of the Dinarides-Alps connection: kinematic and geochronological inferences from the Medvednica Mountains, NE Croatia. Tectonics 34, 1952–1978.
van Gelder, I.E., Willingshofer, E., Sokoutis, D., Cloetingh, S.A.P.L., 2017. The interplay between subduction and lateral extrusion: a case study for the European Eastern Alps based on analogue models. Earth Planet. Sci. Lett. 472, 82–94.
van Unen, M., 2019. Integrating kinematics, mechanics of deformation, thermal modelling and diagenesis in orogenic systems: the Dinarides example. Utrecht Studies in Earth Sciences 191 159 pp, ISBN: 978-90-6266-548-8, PhD Thesis available at. https://dspace.library.uu.nl/handle/1874/380666.
van Unen, M., Matenco, L., Nader, F.H., Darnault, R., Mandic, O., Demir, V., 2019. Kinematics of foreland-vergent crustal accretion: inferences from the Dinarides evolution. Tectonics 38. https://doi.org/10.1029/2018TC005066.
Velaj, T., Davison, I., Serjani, A., Alsop, I., 1999. Thrust tectonics and the role of evaporites in the Ionian Zone of the Albanides. AAPG Bull. 83, 1408–1425.
Vilasi, N., Malandain, J., Barrier, L., Callot, J.-P., Amrouch, K., Guilhaumou, N., Lacombe, O., Muska, K., Roure, F., Swennen, R., 2009. From outcrop and petrographic studies to basin-scale fluid flow modelling: the use of the Albanian natural laboratory for carbonate reservoir characterisation. Tectonophysics 474, 367–392.
Vlahovic, I., Tisljar, J., Velic, I., Maticec, D., 2005. Evolution of the Adriatic Carbonate Platform: palaeogeography, main events and depositional dynamics. Paleogeogr. Paleoclimatol. Paleoecol. 220, 333–360.
Vrabec, M., Fodor, L., 2006. Late Cenozoic tectonics of Slovenia: structural styles at the northeastern corner of the Adriatic microplate. In: Pinter, N., Gyula, G., Weber, J., Stein, S., Medak, D. (Eds.), The Adria Microplate: GPS Geodesy, Tectonics and Hazards. Springer Netherlands, Dordrecht, pp. 151–168.
Vrabec, M., Pavlovcic Preseren, P., Stopar, B., 2006. GPS study (1996–2002) of active deformation along the Paeriadriatic fault system in northeastern Slovenia: tectonic model. Geol. Carpath. 57, 57–65.
Wölfler, A., Kurz, W., Fritz, H., Stüwe, K., 2011. Lateral extrusion in the Eastern Alps revisited: refining the model by thermochronological, sedimentary, and seismic data. Tectonics 30https://doi.org/10.1029/2010tc002782. TC4006.
Wortel, M.J.R., Spakman, W., 2000. Subduction and slab detachment in the Mediteranean-Carpathian region. Science 290, 1910–1917.
Žibret, L., Vrabec, M., 2016. Palaeostress and kinematic evolution of the orogen-parallel nw-se striking faults in the nw external dinarides of Slovenia unraveled by mesoscale fault-slip data analysis. Geol. Croatica 69, 295–305.
Zupanič, J., Babić, L., 2011. Sedimentary evolution of an inner foreland basin margin: Paleogene Promina Beds of the type area, Mt. Promina (Dinarides, Croatia). Geol. Croatica 64, 101–120.